Geochimica et Cosmochimica Acta, Vol. 69, No. 12, pp. 3159–3182, 2005

0016-7037/05 $30.00 + .00

doi:10.1016/j.gca.2005.01.013

Origin of chondritic forsterite grains

ANDREAS PACK,[1,2,*] HERBERT PALME[2] and J. MICHAEL G. SHELLEY[3]

[1]CNRS Centre de Recherches Pétrographiques et Géochimiques, 15 rue Notre Dame des Pauvres, 54501 Vandœuvre-lès-Nancy, France
[2]Institute of Geology and Mineralogy, University of Cologne, Zülpicher Strasse 49b, 50674 Köln, Germany
[3]The Research School of Earth Sciences, The Australian National University, Canberra ACT 0200, Australia

(*Received August* 30, 2004; *accepted in revised form January* 25, 2005)

Abstract—Iron-poor and refractory lithophile element (RLE) rich forsterite grains occur in all major types of unequilibrated chondrites. In our laser ablation inductively coupled mass spectrometry (LA-ICPMS) minor and trace element study we show that refractory forsterites (RF) from carbonaceous (CC), unequilibrated ordinary (UOC) and a Rumuruti chondrite (RC) have similar chemical compositions with high RLE concentrations and low concentrations of Mn, Fe, Co and Ni. Fractionation of RLEs and rare earth elements (REEs) is in agreement with formation by crystallization from a RLE rich silicate melt. Low concentrations and the fractionation of moderately siderophile elements (Fe, Co, Ni) in RFs suggests formation at low oxygen fugacity, possibly in equilibrium with primitive Fe,Ni metal condensates in a gas of solar composition. Anomalously high Ti in the parental melt can be explained by Ti^{3+}/Ti^{4+} ~1.5, supporting formation of RF in highly reducing conditions. Low Mn concentrations indicate formation at high temperatures (>~1160 K). The model of formation of RFs and the accompanying physico-chemical conditions during their formation as well as their relation to non refractory olivine are discussed.

1. INTRODUCTION

The first solids that formed by condensation from a gas of solar composition are refractory minerals rich in Ca, Al and Ti and are suggested to occur in Ca- and Al-rich inclusions (CAI) in unequilibrated chondrites (Grossman, 1972; Ebel and Grossman, 2000). Since CaO, Al_2O_3 and TiO_2 make up less than 5% of the total condensable matter (Lodders, 2003), CAIs are only minor components in chondrites. The most abundant partly or fully condensable elements (by atoms) in a gas of solar composition are O > Fe ≈ Si ≈ Mg which together constitute 84 wt% of a C1 meteorite. Condensation calculations for a gas of solar composition suggest that at a temperature of ~1250 K ($p = 10^{-6}$ bar) these elements condense into olivine and an Fe,Ni-alloy (Ebel and Grossman, 2000), later joined by enstatite. The first olivine condensate would be almost pure forsterite with <0.2 wt% FeO (Palme and Fegley, 1990). Solar nebular Fe,Ni-alloy condensates have been reported from metal rich carbonaceous chondrites (Meibom et al., 1999). FeO-poor RF grains from unequilibrated chondrites may represent the silicate counterpart to the metal condensates (e.g., Weinbruch et al., 2000).

Refractory forsterites were described as minor components from carbonaceous, unequilibrated ordinary and from the highly oxidized Rumuruti chondrites (McSween, 1977; Steele et al., 1985; Steele, 1986a, 1986b; Weinbruch et al., 2000; Bischoff, 2000; Pack et al., 2004). These forsterites are characterized by low fayalite contents (<1% *fa*) and high concentrations of RLEs including Ca, Al, Ti and Sc (Steele et al. 1985; Steele, 1986a, 1986b, 1989; Klerner et al., 2000; Weinbruch et al., 2000). They can be identified by their cathodoluminescence (CL, e.g., Steele, 1985). The abundance of luminescent RF grains was determined by Pack et al. (2004) by area counting to be <0.5 vol.% in CCs and UOCs. Refractory forsterite grains from different types of chondrites are often enriched in ^{16}O with $\Delta^{17}O$ as low as −10‰ (Weinbruch et al., 1993b; Leshin et al., 1997; Pack et al., 2004 and references therein). The oxygen isotope composition of RFs is apparently independent of the isotope ratio of oxygen in the host meteorite. RFs from carbonaceous and ordinary chondrites show similar enrichment in ^{16}O although both groups have very different bulk and chondrule oxygen isotope ratios. RFs from even the most ^{16}O depleted chondrites (Rumuruti chondrites) are ^{16}O rich (Pack et al., 2004; Table 1). Similarities in texture, chemical composition and oxygen isotope ratios of RF grains from the various types of unequilibrated chondrites indicate formation by the same process, possibly from a single nebular reservoir.

Fuchs et al. (1973); Steele (1986a, 1986b) and Weinbruch et al. (2000) suggested that RFs from unequilibrated carbonaceous and ordinary chondrites are remnants of the first generation forsterite condensates. In this respect they are the silicate counterparts to metal condensates. If so, RFs may provide clues to the physical conditions and chemical and isotopic composition of the solar nebula present during growth. Low concentrations of Fe, Co, Ni and Mn are accompanied by enrichment in ^{16}O and support formation of RFs at high temperatures by gas/solid condensation (Palme and Fegley, 1990; Weinbruch et al., 2000). An origin by condensation, however, is not undisputed and other authors (McSween, 1977; Richardson and McSween, 1978; Roedder, 1981; Steele et al., 1985, Jones and Scott, 1989; Jones, 1992) argue that RF formed by crystallization within FeO-poor chondrule melts. The common occurrence of melt inclusions in RF grains from various types of unequilibrated chondrites (Fuchs et al., 1973; McSween, 1977; Roedder, 1981; Steele, 1991; Weinbruch et al., 2000; Pack et al., 2004; this study) supports the origin of RF by crystallization in a silicate melt. Unaltered melt inclusions are rich in Ca, Al and Ti, but generally poor in Mg (~5–7 wt.% MgO). McSween (1977) pointed out that melt inclusions are saturated

* Author to whom correspondence should be addressed (apack@crpg.cnrs-nancy.fr).

Table 1. Major, minor and trace element analyses of RFs. All errors are given as 2σ. Oxygen isotope data are reported relative to SMOW.

Meteorite	Allende (CV3)							
Sample	All3-RF03(a)	All3-RF11(b)	All3-RF11(c)	All3-RF13(a)	All3-RF15(a)	All3-RF16(a)	All3-RF16(b)	All3-RF16(c)
Petrography	isolated RF	RF in chondrule		isolated RF	isolated RF	isolated RF, veinlet with altered glass		
Reference	Pack et al. (2004)	Pack et al. (2004)		This study	This study	Pack et al. (2004), this study		
$\Delta^{17}O$ [‰]†	−5.7	−5.8		n.a.	n.a.	−4.8		
%fa	0.39	0.15	0.29	0.26	0.33	0.21	0.14	0.18
SiO_2* **	43.0	43.1	42.7	43.0	42.9	43.0	43.0	43.0
Al_2O_3	0.229 ± 0.002	0.311 ± 0.002	0.240 ± 0.002	0.287 ± 0.002	0.483 ± 0.010	0.1949 ± 0.0012	0.2289 ± 0.0014	0.252 ± 0.002
CaO	0.636 ± 0.010	0.679 ± 0.012	0.618 ± 0.011	0.523 ± 0.009	0.529 ± 0.014	0.536 ± 0.011	0.605 ± 0.010	0.622 ± 0.012
TiO_2	0.066 ± 0.002	0.084 ± 0.003	0.055 ± 0.002	0.053 ± 0.001	0.114 ± 0.005	0.0510 ± 0.0012	0.0571 ± 0.0013	0.064 ± 0.002
FeO	0.391 ± 0.012	0.151 ± 0.008	0.30 ± 0.02	0.268 ± 0.009	0.32 ± 0.02	0.210 ± 0.007	0.145 ± 0.005	0.185 ± 0.009
Sc	11.9 ± 0.2	26.1 ± 0.3	14.7 ± 0.4	21.0 ± 0.3	19.8 ± 0.5	8.6 ± 0.2	12.5 ± 0.2	16.5 ± 0.2
V	71 ± 2	96.0 ± 1.1	70.8 ± 0.9	153.3 ± 1.3	141 ± 3	35.9 ± 0.5	51.7 ± 0.6	86.3 ± 0.9
Cr	1079 ± 17	544 ± 15	488 ± 8	738 ± 13	1574 ± 53	798 ± 15	612 ± 11	561 ± 12
Mn	93.9 ± 0.8	39 ± 3	36.9 ± 0.7	45.6 ± 0.5	187 ± 6	80 ± 2	44.6 ± 0.5	42.1 ± 0.9
Co	1.21 ± 0.05	0.24 ± 0.02	0.76 ± 0.05	0.52 ± 0.02	0.50 ± 0.06	0.29 ± 0.02	0.19 ± 0.02	0.25 ± 0.02
Ni	2.18 ± 0.14	1.03 ± 0.11	2.7 ± 0.3	1.62 ± 0.12	1.6 ± 0.3	0.90 ± 0.11	0.71 ± 0.10	1.0 ± 0.2
Y	0.38 ± 0.02	0.50 ± 0.03	0.36 ± 0.02	0.45 ± 0.02	0.35 ± 0.04	0.26 ± 0.02	0.29 ± 0.02	0.33 ± 0.02
Zr	0.089 ± 0.010	0.11 ± 0.02	0.062 ± 0.012	0.101 ± 0.014	0.17 ± 0.05	0.046 ± 0.013	0.052 ± 0.009	0.057 ± 0.009
Nb	0.008 ± 0.004	<0.002 −	<0.003 −	0.004 ± 0.003	0.015 ± 0.009	<0.003 −	0.004 ± 0.003	0.003 ± 0.003
La	<0.003 −	<0.002 −	<0.003 −	<0.004 −	<0.003 −	<0.005 −	<0.003 −	<0.004 −
Ce	<0.003 −	<0.003 −	0.003 ± 0.003	0.003 ± 0.002	<0.003 −	<0.003 −	<0.004 −	<0.004 −
Pr	<0.003 −	<0.002 −	<0.002 −	<0.003 −	<0.002 −	<0.002 −	<0.002 −	<0.003 −
Nd	<0.019 −	<0.012 −	<0.013 −	0.013 ± 0.011	0.017 ± 0.039	<0.013 −	<0.017 −	<0.016 −
Sm	0.011 ± 0.011	<0.019 −	0.015 ± 0.014	0.016 ± 0.014	<0.016 −	<0.021 −	<0.017 −	<0.022 −
Eu	<0.004 −	<0.004 −	<0.004 −	<0.005 −	<0.004 −	<0.006 −	<0.005 −	<0.004 −
Gd	0.012 ± 0.009	0.026 ± 0.014	<0.013 −	<0.014 −	0.041 ± 0.027	<0.011 −	<0.015 −	0.019 ± 0.011
Tb	<0.003 −	0.005 ± 0.003	<0.004 −	<0.004 −	<0.004 −	<0.003 −	<0.004 −	0.004 ± 0.004
Dy	0.032 ± 0.014	0.06 ± 0.02	0.021 ± 0.010	0.048 ± 0.014	0.05 ± 0.03	0.033 ± 0.012	0.034 ± 0.012	0.040 ± 0.012
Ho	0.017 ± 0.004	0.017 ± 0.005	0.013 ± 0.004	0.013 ± 0.004	0.013 ± 0.011	0.008 ± 0.004	0.012 ± 0.004	0.011 ± 0.003
Er	0.059 ± 0.014	0.08 ± 0.02	0.057 ± 0.012	0.065 ± 0.016	0.08 ± 0.03	0.038 ± 0.011	0.039 ± 0.012	0.057 ± 0.013
Tm	0.014 ± 0.004	0.021 ± 0.005	0.012 ± 0.004	0.013 ± 0.005	0.010 ± 0.007	0.011 ± 0.003	0.007 ± 0.003	0.012 ± 0.004
Yb	0.112 ± 0.018	0.15 ± 0.02	0.13 ± 0.02	0.11 ± 0.02	0.13 ± 0.04	0.092 ± 0.021	0.089 ± 0.019	0.087 ± 0.017
Lu	0.024 ± 0.005	0.028 ± 0.006	0.013 ± 0.004	0.028 ± 0.007	0.030 ± 0.015	0.015 ± 0.004	0.021 ± 0.005	0.028 ± 0.006

Table 1. (Continued)

Meteorite	Allende (CV3)							Vigarano (CV3)
Sample	All3-RF16(d)	All3-RF16(e)	All3-RF16(f)	AllK1-RF02(a)	AllK1-RF03(a)	AllK1-RF04(a)	AllK1-RF06(a)	Vig1-RF04(a)
Petrography	isolated RF, veinlet with altered glass			isolated RF	isolated RF	isolated RF	isolated RF	isolated RF
Reference	Pack et al. (2004), this study			this study	this study	this study	this study	this study
$\Delta^{17}O$ [‰]†	−4.8			n.a.	n.a.	n.a.	n.a.	n.a.
%fa	0.29	0.14	0.14	0.45	0.69	0.61	0.35	0.34
SiO_2* **	43.0	43.0	43.0	42.0	43.0	43.0	42.0	42.2
Al_2O_3	0.267 ± 0.002	0.300 ± 0.008	0.257 ± 0.003	0.253 ± 0.004	0.394 ± 0.012	0.273 ± 0.003	0.334 ± 0.002	0.255 ± 0.003
CaO	0.660 ± 0.010	0.646 ± 0.012	0.64 ± 0.01	0.675 ± 0.008	0.72 ± 0.02	0.64 ± 0.02	0.562 ± 0.011	0.540 ± 0.012
TiO_2	0.067 ± 0.002	0.073 ± 0.003	0.065 ± 0.002	0.064 ± 0.002	0.077 ± 0.003	0.055 ± 0.002	0.059 ± 0.002	0.054 ± 0.002
FeO	0.30 ± 0.03	0.143 ± 0.005	0.145 ± 0.005	0.45 ± 0.03	0.75 ± 0.04	0.62 ± 0.04	0.36 ± 0.02	0.35 ± 0.04
Sc	19.8 ± 0.2	23.9 ± 0.7	19.3 ± 0.3	10.1 ± 0.2	15.8 ± 0.3	15.2 ± 0.3	7.9 ± 0.2	15.4 ± 0.3
V	118.2 ± 1.1	151 ± 2	131 ± 1	110 ± 2	71.2 ± 1.1	165 ± 4	106.5 ± 1.2	89 ± 3
Cr	518 ± 11	491 ± 11	515 ± 13	927 ± 37	502 ± 13	759 ± 24	678 ± 16	814 ± 37
Mn	44 ± 2	33.1 ± 0.6	38 ± 1	122 ± 6	63.1 ± 1.1	60.8 ± 1.4	44.8 ± 0.7	52 ± 2
Co	0.46 ± 0.05	0.28 ± 0.03	0.25 ± 0.02	0.71 ± 0.06	3.13 ± 0.13	1.68 ± 0.09	0.84 ± 0.05	2.4 ± 0.3
Ni	2.0 ± 0.2	2.5 ± 0.2	0.9 ± 0.1	7.2 ± 0.4	35 ± 2	9.2 ± 0.6	5.4 ± 0.4	61 ± 5
Y	0.37 ± 0.02	0.41 ± 0.02	0.38 ± 0.02	0.42 ± 0.04	0.61 ± 0.03	0.42 ± 0.03	0.50 ± 0.03	0.33 ± 0.03
Zr	0.082 ± 0.013	0.09 ± 0.02	0.07 ± 0.01	0.10 ± 0.02	0.31 ± 0.05	0.13 ± 0.02	0.14 ± 0.02	0.10 ± 0.02
Nb	0.004 ± 0.003	0.004 ± 0.002	0.005 ± 0.003	0.004 ± 0.004	0.016 ± 0.005	0.009 ± 0.005	0.004 ± 0.003	<0.006 −
La	<0.003 −	<0.003 −	<0.002 −	<0.004 −	0.008 ± 0.007	<0.004 −	<0.004 −	<0.005 −
Ce	0.009 ± 0.004	0.027 ± 0.024	<0.002 −	<0.006 −	0.033 ± 0.014	0.005 ± 0.004	<0.003 −	0.006 ± 0.006
Pr	<0.002 −	<0.003 −	<0.002 −	<0.003 −	<0.004 −	<0.004 −	<0.003 −	<0.004 −
Nd	<0.013 −	<0.018 −	<0.012 −	<0.023 −	0.048 ± 0.027	<0.024 −	<0.014 −	<0.025 −
Sm	<0.013 −	<0.018 −	<0.013 −	<0.036 −	<0.021 −	<0.025 −	<0.021 −	<0.032 −
Eu	<0.004 −	<0.005 −	<0.004 −	<0.007 −	<0.007 −	<0.006 −	<0.006 −	<0.009 −
Gd	>0.017 ± 0.010	0.031 ± 0.015	0.017 ± 0.013	<0.019 −	0.024 ± 0.018	0.021 ± 0.016	0.021 ± 0.017	0.022 ± 0.019
Tb	<0.003 −	<0.003 −	<0.003 −	0.009 ± 0.007	0.009 ± 0.006	0.005 ± 0.005	<0.004 −	<0.007 −
Dy	0.049 ± 0.016	0.056 ± 0.014	0.027 ± 0.013	0.046 ± 0.022	0.069 ± 0.028	0.026 ± 0.017	0.060 ± 0.018	0.05 ± 0.04
Ho	0.014 ± 0.004	0.016 ± 0.004	0.016 ± 0.005	0.017 ± 0.007	0.016 ± 0.006	0.017 ± 0.007	0.017 ± 0.006	0.009 ± 0.007
Er	0.066 ± 0.015	0.067 ± 0.015	0.047 ± 0.013	0.049 ± 0.015	0.091 ± 0.024	0.07 ± 0.02	0.075 ± 0.017	0.05 ± 0.02
Tm	0.015 ± 0.004	0.017 ± 0.005	0.013 ± 0.003	0.010 ± 0.004	0.020 ± 0.007	0.012 ± 0.005	0.018 ± 0.006	0.013 ± 0.006
Yb	0.13 ± 0.02	0.147 ± 0.019	0.121 ± 0.020	0.097 ± 0.023	0.187 ± 0.047	0.13 ± 0.04	0.15 ± 0.04	0.12 ± 0.03
Lu	0.026 ± 0.005	0.029 ± 0.006	0.027 ± 0.006	0.026 ± 0.008	0.028 ± 0.009	0.025 ± 0.007	0.022 ± 0.007	0.026 ± 0.011

Table 1. (Continued)

Meteorite	Vigarano (CV3)				Murchison (CM2)			
Sample Petrography	Vig1-RF05(a) RF in chondrule fragment, spinel inclusion	Vig1-RF06(a) isolated RF, glass inclusions	Vig1-RF06(b)	Vig1-RF10(a) RF in chondrule fragment	Mur-RF01(a) isolated RF	Mur-RF05(a) isolated RF	Mur-A(a) isolated FeO-rich olivine	Mur-C(a) isolated FeO-rich olivine
Reference	this study	this study		this study	this study	Pack et al.	this study	this study
$\Delta^{17}O$ [‰][†]	n.a.	n.a.		n.a.	n.a.	+2.5	n.a.	n.a.
%fa	0.17	0.16	0.15	0.14	0.39	0.10	37.6	35.8
SiO_2* **	42.5	42.9	42.9	42.3	42.8	43.0	36.4	37.2
Al_2O_3	0.262 ± 0.003	0.362 ± 0.006	0.301 ± 0.003	0.280 ± 0.002	0.224 ± 0.002	0.206 ± 0.004	0.0118 ± 0.0002	0.0379 ± 0.0008
CaO	0.671 ± 0.014	0.67 ± 0.02	0.667 ± 0.013	0.638 ± 0.011	0.38 ± 0.01	0.65 ± 0.01	0.055 ± 0.004	0.199 ± 0.015
TiO_2	0.054 ± 0.002	0.081 ± 0.004	0.063 ± 0.002	0.066 ± 0.003	0.055 ± 0.002	0.066 ± 0.002	0.0010 ± 0.0001	0.0032 ± 0.0004
FeO	0.18 ± 0.02	0.17 ± 0.03	0.15 ± 0.02	0.142 ± 0.010	0.39 ± 0.02	0.095 ± 0.004	29.6 ± 1.3	30.3 ± 2.8
Sc	10.3 ± 0.3	23.8 ± 0.4	17.6 ± 0.3	18.0 ± 0.4	11.5 ± 0.1	11.1 ± 0.4	1.6 ± 0.1	4.1 ± 0.3
V	107.9 ± 1.3	132 ± 2	98 ± 2	75 ± 2	100 ± 1	54 ± 2	21 ± 0	38 ± 1
Cr	609 ± 27	544 ± 27	537 ± 20	432 ± 13	1165 ± 19	528 ± 9	2432 ± 60	2538 ± 113
Mn	38.2 ± 1.1	35.5 ± 0.9	26.9 ± 0.3	27.4 ± 0.6	98 ± 2	43 ± 1	2372.4 ± 34.2	2772.2 ± 67.1
Co	0.43 ± 0.05	0.43 ± 0.05	0.39 ± 0.02	0.29 ± 0.08	0.94 ± 0.06	0.16 ± 0.02	272.5 ± 3.8	184.7 ± 3.8
Ni	1.45 ± 0.14	2.1 ± 0.3	1.34 ± 0.11	3 ± 2	3.4 ± 0.3	1.1 ± 0.2	631.53 ± 12.19	290.00 ± 10.04
Y	0.43 ± 0.03	0.47 ± 0.04	0.40 ± 0.02	0.41 ± 0.03	0.29 ± 0.01	0.30 ± 0.02	0.018 ± 0.005	0.053 ± 0.010
Zr	0.09 ± 0.02	0.15 ± 0.02	0.08 ± 0.02	0.08 ± 0.02	0.06 ± 0.01	0.06 ± 0.01	0.012 ± 0.007	0.017 ± 0.009
Nb	<0.004 −	<0.004 −	0.004 ± 0.003	0.005 −	0.008 ± 0.003	0.003 ± 0.002	0.010 ± 0.005	0.011 ± 0.005
La	<0.005 −	<0.005 −	<0.004 −	0.005 −	0.001 ± 0.002	0.002 ± 0.002	<0.003 −	<0.004 −
Ce	<0.005 −	<0.006 −	<0.003 −	0.005 −	0.001 ± 0.001	0.003 ± 0.002	<0.004 ± 0.00	<0.005 −
Pr	<0.003 −	<0.004 −	<0.003 −	<0.004 −	<0.001 −	<0.001 −	<0.004 −	<0.004 −
Nd	<0.029 −	<0.027 −	<0.023 −	<0.021 −	<0.003 −	0.003 ± 0.006	<0.019 −	<0.019 −
Sm	<0.029 −	<0.025 −	<0.021 −	0.02 ± 0.02	0.003 ± 0.007	0.004 ± 0.008	<0.033 −	<0.028 −
Eu	<0.010 −	<0.007 −	<0.006 −	0.008 ± 0.006	0.002 ± 0.002	<0.001 −	<0.007 −	<0.008 −
Gd	<0.029 −	<0.020 −	0.020 ± 0.017	<0.015 −	0.006 ± 0.006	<0.007 ± 0.007	<0.017 −	<0.017 −
Tb	<0.007 −	0.007 ± 0.006	<0.005 −	<0.006 −	0.003 ± 0.002	<0.001 −	0.006 −	0.007 −
Dy	0.05 ± 0.02	0.08 ± 0.04	0.051 ± 0.019	0.049 ± 0.019	0.029 ± 0.010	0.038 ± 0.011	<0.014 −	<0.016 ± 0.02
Ho	0.012 ± 0.006	0.021 ± 0.008	0.015 ± 0.004	0.007 ± 0.005	0.012 ± 0.003	0.012 ± 0.003	0.004 −	0.004 −
Er	0.06 ± 0.02	0.07 ± 0.03	0.053 ± 0.015	0.059 ± 0.018	0.041 ± 0.009	0.049 ± 0.011	<0.014 −	<0.013 −
Tm	0.011 ± 0.007	0.023 ± 0.008	0.018 ± 0.005	0.011 ± 0.005	0.009 ± 0.003	0.012 ± 0.003	<0.005 −	<0.004 −
Yb	0.12 ± 0.03	0.21 ± 0.05	0.15 ± 0.03	0.16 ± 0.03	0.073 ± 0.014	0.096 ± 0.017	0.014 −	0.020 ± 0.016
Lu	0.026 ± 0.009	0.035 ± 0.011	0.024 ± 0.006	0.033 ± 0.009	0.014 ± 0.004	0.017 ± 0.005	0.01 −	0.01 −

Table 1. (Continued)

Meteorite	Murchison (CM2)		Chainpur (LL3.4)					
Sample	Mur-E(a) isolated	Mur-G(a) isolated	Cha-CH01(a)	Cha-CH01(b)	Cha-CH01(c)	Cha1-CH01(b)	Cha1-A(a)	Cha1-A(c)
Petrography	FeO-rich olivine	FeO-rich olivine	RF in chondrule, spinel inclusions			RF in chondrule	FeO-rich chondrule olivine	
Reference	this study	this study	Pack et al. (2004)			Pack et al. (2004)	this study	
$\Delta^{17}O$ [‰]†	n.a.	n.a.	−5.7			+1.7	n.a.	
%fa	32.8	39.6	0.17	0.17	0.34	0.60	11.8	12.8
SiO_2* **	37.1	36.5	42.7	42.7	42.7	42.5	40.2	40.2
Al_2O_3	0.0128 ± 0.0003	0.0425 ± 0.0007	0.307 ± 0.002	0.270 ± 0.006	0.342 ± 0.002	0.293 ± 0.005	0.0116 ± 0.0002	0.0135 ± 0.0008
CaO	0.066 ± 0.006	0.170 ± 0.008	0.636 ± 0.013	0.64 ± 0.02	0.614 ± 0.008	0.491 ± 0.013	0.030 ± 0.004	0.080 ± 0.004
TiO_2	0.0015 ± 0.0002	0.0031 ± 0.0003	0.078 ± 0.003	0.073 ± 0.004	0.083 ± 0.002	0.055 ± 0.002	0.00106 ± 0.00008	0.0028 ± 0.0003
FeO	29 ± 5	34 ± 4	0.168 ± 0.007	0.175 ± 0.013	0.34 ± 0.02	0.62 ± 0.04	11.4 ± 0.6	12.4 ± 0.7
Sc	2.25 ± 0.07	3.63 ± 0.13	24.8 ± 0.4	22.7 ± 0.7	25.9 ± 0.4	19.1 ± 0.4	2.39 ± 0.09	2.91 ± 0.13
V	44.7 ± 1.1	33.4 ± 1.0	218 ± 3	207 ± 3	222 ± 2	175 ± 2	41.6 ± 0.8	51.4 ± 1.1
Cr	3015 ± 203	2521 ± 131	460 ± 11	464 ± 11	458 ± 7	782 ± 22	1184 ± 44	887 ± 33
Mn	1886 ± 51	2649 ± 54	24.0 ± 0.4	25.5 ± 0.5	28.4 ± 0.3	72 ± 2	2394 ± 34	2495 ± 33
Co	184 ± 4	299 ± 7	0.28 ± 0.03	0.28 ± 0.04	3.2 ± 0.3	0.46 ± 0.09	24.8 ± 0.3	25.6 ± 0.5
Ni	480 ± 23	521 ± 20	1.07 ± 0.14	0.99 ± 0.13	77 ± 6	2.4 ± 0.2	38.8 ± 0.7	39.7 ± 1.0
Y	0.030 ± 0.012	0.060 ± 0.010	0.36 ± 0.03	0.35 ± 0.04	0.41 ± 0.03	0.33 ± 0.02	0.021 ± 0.007	0.032 ± 0.009
Zr	0.014 ± 0.011	0.011 ± 0.006	0.10 ± 0.02	0.14 ± 0.03	0.17 ± 0.02	0.074 ± 0.014	0.010 ± 0.008	0.017 ± 0.009
Nb	0.011 ± 0.007	0.012 ± 0.005	0.003 ± 0.004	0.003 ± 0.005	0.008 ± 0.004	<0.005 −	0.005 ± 0.004	0.006 ± 0.004
La	<0.006 −	<0.005 −	<0.209 −	0.003 ± 0.003	0.009 ± 0.003	0.006 ± 0.004	<0.003 −	<0.005 −
Ce	<0.005 −	<0.004 −	<0.167 −	<0.118 −	0.016 ± 0.006	0.012 ± 0.005	<0.004 −	<0.004 −
Pr	<0.005 −	<0.003 −	<0.166 −	<0.188 −	0.003 ± 0.002	<0.003 −	<0.004 −	<0.004 −
Nd	<0.023 −	<0.021 −	<0.149 −	<0.137 −	0.014 ± 0.011	<0.028 −	<0.017 −	<0.025 −
Sm	<0.034 −	<0.029 −	<0.176 −	<0.293 −	<0.175 −	0.026 ± 0.025	<0.026 −	<0.026 −
Eu	<0.008 −	<0.007 −	<0.133 −	<0.188 −	<0.163 −	0.007 ± 0.005	<0.006 −	<0.007 −
Gd	<0.021 −	<0.020 −	0.025 ± 0.017	<0.295 −	0.014 ± 0.010	<0.014 −	<0.014 −	<0.021 −
Tb	0.007 −	0.006 −	<0.138 −	<0.195 −	0.004 ± 0.003	<0.005 −	<0.005 −	<0.006 −
Dy	<0.018 −	<0.017 −	0.040 ± 0.015	0.04 ± 0.02	0.041 ± 0.013	0.030 ± 0.016	<0.014 −	<0.015 −
Ho	0.004 −	0.007 ± 0.004	0.014 ± 0.007	0.014 ± 0.006	0.016 ± 0.004	0.008 ± 0.003	<0.004 −	<0.004 −
Er	<0.020 −	0.015 ± 0.012	0.08 ± 0.02	0.030 ± 0.017	0.064 ± 0.014	0.051 ± 0.016	<0.02 −	<0.012 −
Tm	<0.006 −	0.005 ± 0.006	0.010 ± 0.004	0.013 ± 0.005	0.012 ± 0.003	0.013 ± 0.004	0.005 ± 0.004	<0.003 −
Yb	0.020 −	0.021 ± 0.012	0.16 ± 0.03	0.14 ± 0.03	0.13 ± 0.02	0.11 ± 0.02	<0.011 −	<0.012 −
Lu	0.01 ± 0.01	<0.005 −	0.024 ± 0.007	0.028 ± 0.009	0.024 ± 0.004	0.021 ± 0.008	<0.004 −	<0.005 −

Table 1. (Continued)

Meteorite	Chainpur (LL3.4)			Dar al Gani 369 (L/H3)			Dar al Gani 378 (H/L3)
Sample	Cha1-B(a)	Cha1-B(b)	Cha1-B(c)	DaG369-RF02(e)	DaG369-RF06(a)	DaG369-RF06(b)	DaG378-RF01(a)
Petrography		FeO-rich chondrule olivine		RF in chondrule, partly altered glass inclusion	isolated RF, metal inclusion		RF in chondrule fragment
Reference	this study			Pack et al. (2004)	this study		this study
$\Delta^{17}O$ [‰]†	n.a.			0.0	−3.8		n.a.
%fa	8.6	14.6	11.3	0.31	0.70	0.36	0.81
SiO_2* **	41.0	40.2	40.9	42.7	42.7	42.7	42.9
Al_2O_3	0.0283 ± 0.0008	0.0163 ± 0.0002	0.0210 ± 0.0002	0.26 ± 0.05	0.351 ± 0.006	0.338 ± 0.004	0.308 ± 0.009
CaO	0.062 ± 0.004	0.067 ± 0.004	0.090 ± 0.005	0.40 ± 0.02	0.63 ± 0.02	0.74 ± 0.02	0.64 ± 0.02
TiO_2	0.0029 ± 0.0002	0.00195 ± 0.00012	0.0029 ± 0.0002	0.043 ± 0.002	0.056 ± 0.002	0.0536 ± 0.0014	0.104 ± 0.004
FeO	8.5 ± 0.4	14.0 ± 0.7	11.0 ± 0.5	0.29 ± 0.10	0.70 ± 0.06	0.35 ± 0.03	0.8 ± 0.2
Sc	2.43 ± 0.08	2.67 ± 0.12	2.47 ± 0.08	4.2 ± 0.3	12.9 ± 0.2	2.25 ± 0.11	28.2 ± 0.4
V	31.6 ± 0.3	31.6 ± 0.5	15.9 ± 0.2	69 ± 2	103.5 ± 1.3	52.7 ± 0.9	111 ± 2
Cr	1792 ± 40	682 ± 17	853 ± 23	692 ± 71	543 ± 16	512 ± 12	573 ± 22
Mn	1613 ± 11	2550 ± 30	2039 ± 18	49 ± 2	35.8 ± 1.0	49 ± 2	93 ± 8
Co	25.4 ± 0.3	31.5 ± 0.5	26.8 ± 0.3	1.5 ± 0.3	25 ± 2	20 ± 2	0.48 ± 0.07
Ni	48.4 ± 1.0	30.2 ± 0.7	47.6 ± 1.0	8 ± 2	319 ± 19	426 ± 29	2.9 ± 0.8
Y	0.038 ± 0.007	0.038 ± 0.007	0.030 ± 0.007	0.36 ± 0.05	0.42 ± 0.03	0.54 ± 0.03	0.50 ± 0.04
Zr	0.018 ± 0.008	0.009 ± 0.006	0.007 ± 0.006	0.34 ± 0.11	0.13 ± 0.02	0.47 ± 0.05	0.17 ± 0.03
Nb	0.008 ± 0.004	0.004 ± 0.004	0.004 ± 0.003	0.015 ± 0.012	0.009 ± 0.004	0.014 ± 0.007	<0.04 −
La	<0.003 −	<0.003 −	<0.003 −	<0.013 −	0.004 ± 0.005	0.028 ± 0.010	<0.02 −
Ce	<0.003 −	<0.003 −	<0.003 −	0.05 ± 0.03	0.009 ± 0.004	0.045 ± 0.010	<0.03 −
Pr	<0.002 −	<0.003 −	<0.003 −	<0.01 −	<0.005 −	<0.005 −	<0.02 −
Nd	<0.015 −	<0.015 −	<0.019 −	<0.08 −	<0.020 −	0.04 ± 0.03	<0.1 −
Sm	<0.019 −	<0.021 −	<0.014 −	<0.05 −	<0.031 −	<0.02 −	<0.1 −
Eu	<0.005 −	<0.004 −	<0.004 −	<0.02 −	0.007 ± 0.006	<0.009 −	<0.05 −
Gd	<0.015 −	<0.014 −	<0.012 −	<0.05 −	<0.024 −	<0.02 −	<0.1 −
Tb	0.004 ± 0.003	<0.004 −	<0.004 −	<0.02 −	0.008 ± 0.005	0.007 ± 0.006	<0.03 −
Dy	<0.013 −	<0.013 −	0.017 ± 0.011	0.06 ± 0.06	0.04 ± 0.02	0.04 ± 0.02	<0.09 −
Ho	<0.003 −	0.004 ± 0.003	<0.004 −	<0.01 −	0.012 ± 0.006	0.015 ± 0.007	<0.02 −
Er	<0.01 −	0.015 ± 0.009	0.010 ± 0.009	0.05 ± 0.02	0.05 ± 0.02	0.068 ± 0.02	0.077 ± 0.02
Tm	<0.003 −	<0.003 −	<0.003 −	<0.01 −	0.014 ± 0.007	0.024 ± 0.007	<0.02 −
Yb	0.011 ± 0.008	0.013 ± 0.011	<0.010 −	<0.05 −	0.13 ± 0.03	0.13 ± 0.04	0.15 ± 0.04
Lu	0.004 ± 0.003	<0.004 −	0.004 ± 0.003	<0.01 −	0.021 ± 0.009	0.023 ± 0.007	0.041 ± 0.011

Table 1. (Continued)

Meteorite	Dar al Gani 378 (H/L3)		Dar al Gani 013 (R3-5)	
Sample	DaG378-RF01(c)	DaG378-RF03(b)	DaG013-RF08(a)	DaG013-RF10(a)
Petrography	RF in chondrule fragment	RF in chondrule fragment	isolated RF	isolated RF
Reference	this study	Pack et al. (2004)	Pack et al. (2004)	Pack et al. (2004)
$\Delta^{17}O$ [‰]†	n.a.	+2.3	−4.0	−6.5
%fa	1.33	0.64	0.76	0.31
SiO_2* **	42.6	42.7	42.9	43.5
Al_2O_3	0.540 ± 0.012	0.336 ± 0.004	0.212 ± 0.008	0.426 ± 0.007
CaO	0.65 ± 0.02	1.58 ± 0.10	0.57 ± 0.03	0.66 ± 0.02
TiO_2	0.141 ± 0.006	0.055 ± 0.002	0.046 ± 0.002	0.098 ± 0.004
FeO	1.4 ± 0.13	0.66 ± 0.11	0.78 ± 0.06	0.32 ± 0.02
Sc	39.7 ± 1.1	20.1 ± 0.5	1.76 ± 0.11	13.9 ± 0.5
V	142 ± 4	350 ± 6	17.6 ± 0.5	34.2 ± 1.1
Cr	518 ± 20	841 ± 36	627 ± 66	398 ± 20
Mn	79 ± 6	68 ± 11	123 ± 45	35.0 ± 1.1
Co	69 ± 5	14.0 ± 0.5	17 ± 3	4.2 ± 0.4
Ni	1350 ± 110	355 ± 14	119 ± 28	32 ± 3
Y	0.75 ± 0.05	0.40 ± 0.04	0.39 ± 0.03	0.48 ± 0.04
Zr	0.33 ± 0.06	0.22 ± 0.03	0.12 ± 0.02	0.24 ± 0.03
Nb	<0.03 −	<0.03 −	0.009 ± 0.015	<0.005 −
La	<0.02 −	<0.02 −	<0.005 −	<0.006 −
Ce	0.047 ± 0.011	<0.02 −	<0.006 −	<0.007 −
Pr	<0.01 −	<0.01 −	<0.004 −	<0.004 −
Nd	<0.1 −	<0.1 −	<0.029 −	<0.026 −
Sm	<0.1 −	<0.1 −	0.02 ± 0.02	<0.038 −
Eu	<0.04 −	<0.04 −	<0.008 −	<0.010 −
Gd	<0.1 −	<0.08 −	0.024 ± 0.015	0.05 ± 0.03
Tb	<0.02 −	<0.02 −	<0.005 −	<0.008 −
Dy	<0.09 −	<0.09 −	0.05 ± 0.03	0.03 ± 0.02
Ho	0.027 ± 0.009	<0.02 −	0.016 ± 0.008	0.014 ± 0.011
Er	0.124 ± 0.04	<0.08 −	0.06 ± 0.02	0.08 ± 0.04
Tm	<0.02 −	<0.02 −	0.017 ± 0.005	0.024 ± 0.009
Yb	0.22 ± 0.04	0.09 ± 0.03	0.09 ± 0.03	0.14 ± 0.06
Lu	0.05 ± 0.02	0.029 ± 0.010	0.018 ± 0.008	0.019 ± 0.012

* EPMA data; ** all data in ppm, except Si, Al, Ca, Ti and Fe in wt.% of the oxides; † data from Pack et al. (2004), n.a.: not analyzed

in anorthite but not in olivine. This would imply disequilibrium between olivine hosts and melt inclusions. McSween (1977) concluded that olivine crystallizes beyond its stability field because of the hampered formation of stable anorthite crystallization seeds. Hence, glass inclusions in RFs represent highly evolved residual melts from which the olivine component was removed. They are in metastable equilibrium with their host olivine grains (McSween, 1977).

Recently, Varela et al. (2002); Pack and Palme (2003) and Pack et al. (2004) suggested that RF formed in association with refractory melt condensates. This model was briefly discussed in earlier works by Fuchs et al. (1973) and Weinbruch et al. (2000) to explain the occurrence of melt inclusions in RF grains.

Chondrules formed by melting of preexisting solid material in one or more brief, but intense heating events (Wasson and Rubin, 2003). In contrast, melt condensates form by gas to liquid condensation and not by melting of preexisting material (Ebel and Grossman, 2000). RF grains that formed by crystallization in association with melt condensates should include information about the chemical and isotopic composition of the solar nebula. If RFs, however, crystallized within chondrules they would only reflect the composition of the chondrule melt, possibly modified by the nebular environment (e.g., Tissandier et al., 2002).

In this study we have analyzed minor and trace elements in RF from different types of chondrites (CC, UOC, RC) using LA-ICPMS. We primarily concentrate on two questions: (*a*) do RFs from different types of chondrites show any compositional characteristics that may relate them to their host meteorites and (*b*) is their composition indicative of either formation by crystallization from a melt or by condensation from a gas phase?

2. ANALYTICAL PROCEDURES

Petrographic work was performed on polished sections by means of optical microscopy, back scattered electron (BSE) imaging and CL microscopy. BSE and CL imaging was conducted using a JEOL 8900 RL electron microprobe (University of Cologne). The same probe was used for major and minor element electron probe micro analyses (EPMA). After petrographic studies and EPMA, minor and trace elements were determined by LA-ICPMS at the RSES of the Australian National University in Canberra using an Aligent 7500s ICP-MS. Sample material was ablated in helium atmosphere in a two volume cell using a 193 nm ArF excimer laser with aperture imaging optics. Spot diameters were between 32 and 56 μm. Analyses were normalized to the concentration of Si previously determined at each site by EPMA. Elements were calibrated using NIST 612 glass with concentration values by Pearce et al. (1997) and Norman et al. (1996, Y, Zr). Ti and Fe were calibrated using two standards (NIST 612 and USGS BCR-2G basaltic glass, concentration data from Rocholl, 1998). Errors were calculated according to the procedure described by Longerich et al. (1996). 2σ errors are reported throughout the manuscript, in the table and figures.

3. SAMPLING AND PETROGRAPHY

RF grains were identified by their CL on carbon coated polished thin sections. RFs were identified in sections of

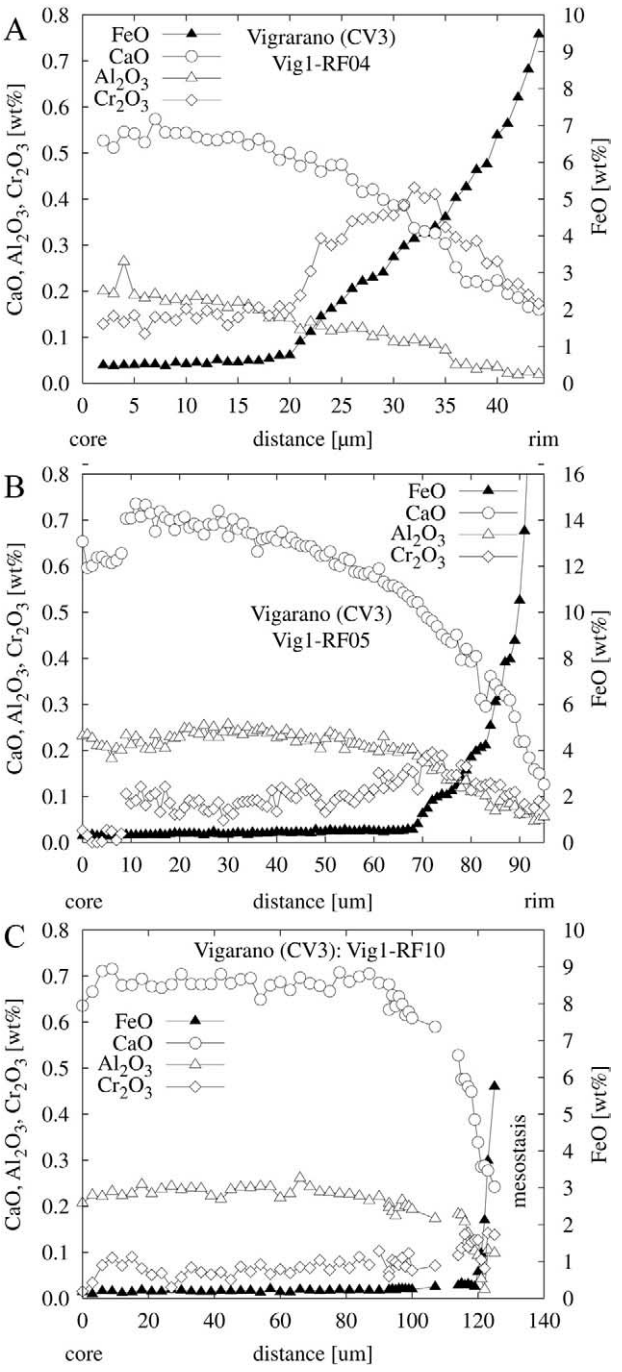

Fig. 1. EPMA profiles across RF grains Vig1-RF04 (A), Vig1-RF05 (B) and Vig1-RF10 (C) from Vigarano.

Murchison (CM2), Allende (CV3), Vigarano (CV3), Chainpur (LL3.4), Dar al Gani 369 (L/H3), Dar al Gani 378 (H/L3) and Dar al Gani 013 (R3.5–6). Details about sampling, definition and abundance of RF grains are given by Pack et al. (2004). RF grains occur as isolated grains in the matrix and as relict grains in chondrules or chondrule fragments. About half of the grains that were analyzed in this study were previously petrographically described by Pack et al. (2004). For those grains, only a brief petrographic description is given (Table 1). For all other

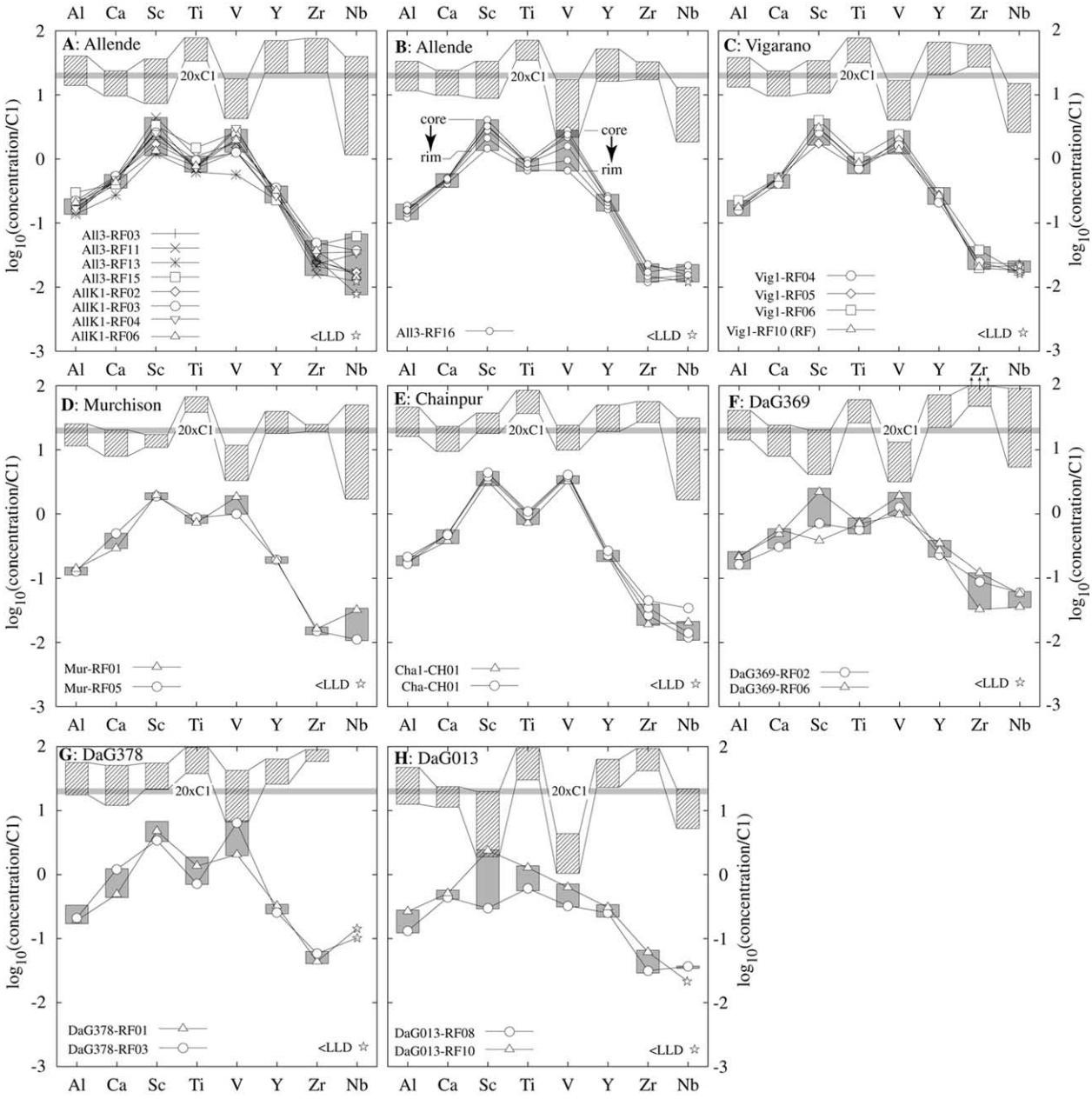

Fig. 2. C1-normalized RLE concentrations of RFs from carbonaceous chondrites Allende (A, B), Vigarano (C), and Murchison (D), from ordinary chondrites Chainpur (E), Dar al Gani 369 (F) and Dar al Gani 378 (G) and from Rumuruti chondrite Dar al Gani 013 (H). The diagonally hatched boxes indicate the composition of a silicate melt in equilibrium with RF (filled boxes).

grains, petrography and positions of LA-ICPMS spots are shown in BSE and corresponding CL images in the Appendix (App. Figs. 1–3). Some of the studied olivine grains were previously analyzed for oxygen isotopes (Pack et al., 2004). For those grains, mean $\Delta^{17}O$ values are reported in Table 1. They vary in the range of $-6.5 < \Delta^{17}O < +2.5‰$.

RF grains from the different types of chondrites are up to ~0.5 mm in diameter (Pack et al., 2004). RF grains exhibit CL emission, which distinguishes them from non-refractory, low-FeO olivine. CL is highest in the cores and vanishes towards the more ferrous rims. RF grains are often cross cut by cracks that appear dark in CL due to the more ferrous composition of the olivine adjacent to the cracks (e.g., App. Fig. 2A,B). The thickness of the outer ferrous rims varies from meteorite to meteorite, but also within a single meteorite and even between different sides of a single RF grain (App. Fig. 1I). Only RF grains from Murchison (CM2) either lack any ferrous rims or have extremely thin ferrous surroundings (App. Fig. 3A; Pack et al., 2004, therein Fig. 10C and E).

Pack and Palme (2003) and Pack et al. (2004) have shown that high CL intensity is caused by low Fe and high concentrations of Al and especially Ti. Olivine with low concentra-

tions of Fe and low concentrations of Al and Ti does not show CL emission. Figures App. 1–3 reveal differences in CL emission in a single grain. The absolute CL intensity is highly variable, but was not quantified with the CL detector. Steele et al. (1985) and Steele (1986a, 1986b) showed that the CL color varies between blue and orange. He noted that blue regions show the highest RLE concentrations. Since we used a black and white CL detection unit, we cannot give any information regarding the CL color.

Isolated RF grains do not show any associations with other minerals (e.g., clinopyroxene) except occasions of inclusions of glass (Fig. 3 and App. Fig. 2G), spinel (App. Fig. 2E) and metal and small amounts of low-Ca pyroxene along their outer rims (App. Fig. 2E). A total of 31 RF grains were described by Pack et al. (2004) and in this study. Four (13%) contain spinel inclusions, four (13%) metal inclusions, three (10%) glass inclusions and 20 (64%) no inclusions. Spinel inclusions are solid solutions between Mg-Al-spinel and hercynite with hercynite contents ranging from 2 (Mur-RF07, Pack et al., 2004) to 31 mol% (Vig-RF16, Pack et al., 2004), respectively. The spinel inclusion in RF Vig-RF05 (App. Fig. 2E) contains 25.5 mol% hercynite whereas the olivine host contains only 0.55 mol% fayalite. Inclusions of spinel in RFs were also reported by Steele (1986a, 1986b).

4. MINERAL CHEMISTRY

RF grains are poor in FeO (~0.15–1 wt.%) with high concentrations of Ca, Al and Ti. EPMA profiles were measured across three RF grains from Vigarano (Vig-RF04, Vig-RF05, Vig1-RF10, App. Fig. 2C, E and I). Similar to the observations by Pack and Palme (2003) and Pack et al. (2004), concentrations of Ca and Al either decrease from core to rim (Fig. 1A and B) or are constant throughout the grains (Fig. 1C). None of the grains studied here and of those described by Pack and Palme (2003) and Pack et al. (2004) show an increase in Ca and Al from core towards the rims. Concentrations of Fe increase towards the non-luminous rims, typically with an abrupt increase between core and rim (Fig. 1A and B). RF grain Vig1-RF04 (Fig. 1A) shows a distinct increase in Cr between Fe-poor core and Fe-rich rim. A similar behavior of Cr was described by Pack et al. (2004) from RF from Rumuruti chondrite Dar al Gani 013 (R3.5–6). Weinbruch et al. (1990) identified inclusions of Cr-rich spinel at the interface between Fe-poor cores and surrounding Fe-rich rims in olivine grains from Allende (CV3). They suggest that spinel inclusions at the core to rim boundary formed at high temperatures under oxidizing conditions. Since Al is not correlated with Cr at the core to rim interface of Vig1-RF04, we suggest that Cr may be hosted by submicroscopic inclusions of a magnesio-chromite ($[Mg,Fe]Cr_2O_4$).

Results of LA-ICPMS analyses of RFs and of a few non-refractory, isolated and chondrule olivine grains from CCs, UOCs and one RC are listed in Table 1. Four groups of minor and trace elements in RF will be discussed separately: (*a*) RLEs, (*b*) and REEs, (*c*) the group of common lithophile elements (Cr, Mn) and (*d*) the group of moderately siderophile elements (Fe, Co, Ni). Concentrations of minor and trace elements are displayed normalized to the concentrations in C1 meteorites taken from the compilation by Lodders (2003).

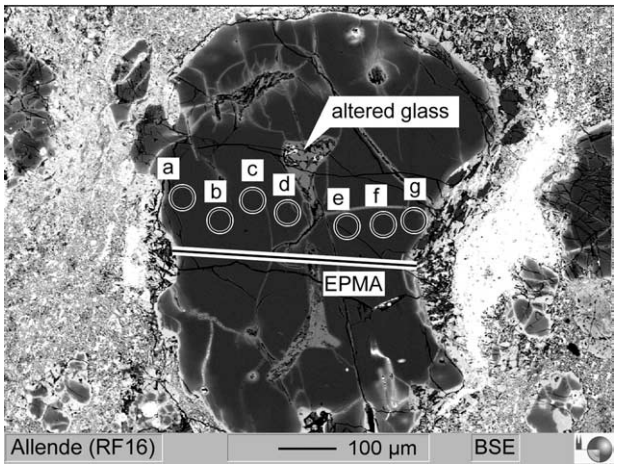

Fig. 3. Luminescent RF from Allende (All3-RF16). Positions of LA-ICPMS spots (a–g, see Fig. 4) along an EPMA profile are indicated (modified after Pack et al., 2004).

4.1. RLEs

Refractory lithophile elements Al, Ca, Sc, Ti, V, Y, Zr and Nb are similarly enriched in RFs from different types of chondrites (Table 1) and show very similar C1-normalized fractionation patterns (Fig. 2A–H). Typical RLE concentrations in RFs are 0.3 wt% Al_2O_3, 0.7 wt% CaO and 600 ppm TiO_2 (Table 1). The lowest C1-normalized RLE concentrations show Zr and Nb with 0.01–0.1×C1. Our Sc concentration data (~10–25 ppm) are in good agreement to the data reported by Weinbruch et al. (2000; 7–17 ppm).

It was pointed out by Pack and Palme (2003) and Pack et al. (2004), but is also shown here (Fig. 1A–C) that RLE concentrations in many RFs systematically decrease from core to rim. All3-RF16 (Fig. 3) is an unusually large RF grain from Allende that allowed the measurement of a traverse by means of LA-ICPMS (Fig. 4A–). The traverse was analyzed parallel to an EPMA profile that was previously measured by Pack and Palme (2003; Fig. 4A). Ca, Al, Ti, Sc, V, Y and Zr systematically decrease from core to rim (Fig. 4B–F). The relative decrease from core to rim varies between 17% for Ca and 76% for V with an average relative decrease of ~50%.

4.2. REEs

REEs in olivine are generally low due to their incompatibility with the olivine structure. All RF grains show a systematic LREE < HREE fractionation relative to the composition of the C1 meteorites (Fig. 5A–H). RFs from different types of chondrites all have very similar fractionated REEs with the C1-normalized concentration decreasing from Lu towards La. Lu reaches 0.03 ppm, which is 1.3× the chondritic value. Although not a REE, Y^{3+} behaves very similarly to Ho^{3+} in most geological processes and is therefore also displayed in the REE plots in Figure 5. A similar behavior of Y and Ho is observed in RFs. Due to the limitations of the LA-ICPMS, duration of a

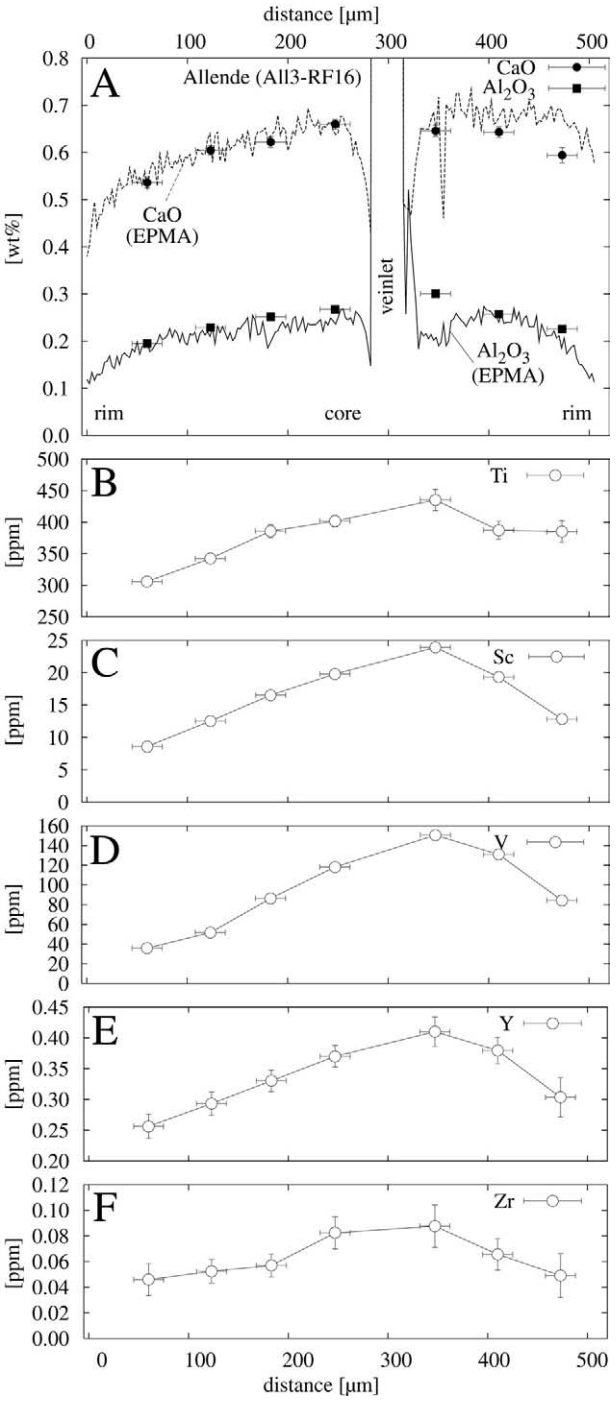

Fig. 4. Chemical profiles (EPMA [A] and LA-ICPMS [B-F]) across RF All3-RF16 from Allende (see Fig. 3). EPMA data are from Pack and Palme (2003).

stable signal and spot size, respectively, concentrations of REEs lighter than ~Dy are mostly below detection limit or have large errors. Extrapolating the trend of decreasing C1-normalized REE abundance from Lu to La would give a La concentration in the range of $\sim 10^{-4}\times$C1 (~0.023 ppb). With respect to REE fractionation, our data are in disagreement to the data reported by Weinbruch et al. (2000) who report largely unfractionated C1-normalized REEs with La/Lu = 0.3 in RF grains from Allende. Since our data on light REEs are mostly below the detection limit, we cannot decide whether there is a negative Eu anomaly in RF grains, such as reported by Weinbruch et al. (2000, Eu/Eu* = 0.3).

4.3. Cr and Mn

Concentrations of Cr vary between 400 and 1000 ppm and of Mn between 25 and 100 ppm, respectively. Cr and Mn exhibit a weak positive correlation with a lower limit at 400 ppm Cr and 24 ppm Mn with Mn correlating with Fe towards the more ferrous rims. Most RF core analyses cluster at ~500 ppm Cr and ~40 ppm Mn. Cr is often enriched at the interface between luminescent core and ferrous rims (Fig. 1A and B). In RFs Vig1-RF04 and Vig1-RF05, no correlation between Cr and Al is observed (Fig. 1A and B). Weinbruch et al. (2000) report minimum Mn concentrations in RF grains from Allende of 30–40 ppm.

4.4. Fe, Co and Ni

The C1-normalized abundances of Fe, Co and Ni are systematically fractionated in RFs with Fe > Co > Ni (Fig. 6A–H). The lowest FeO concentration was measured in RF All3-RF16 from Allende with 0.15 wt% ($6.4\times10^{-3}\times$C1, Fig. 3B, Table 1). The same RF grain shows the lowest concentrations of Co (0.19 ppm, $3.8\times10^{-4}\times$C1) and Ni (0.7 ppm, $6.6\times10^{-5}\times$ C1). A few grains show higher concentrations of Co and Ni and only little or no fractionation amongst Fe, Co and Ni relative to C1. Weinbruch et al. (2000) reported minimum concentrations of Ni of 1.4–1.7 ppm.

4.5. Comparison of RF with Non-Refractory Chondrite Olivine Grains

To demonstrate the difference in chemical composition between RFs and non-refractory, more ferrous chondrite olivine, we have analyzed four isolated ferrous olivine grains from Murchison (CM2) and three olivine phenocrysts from Chainpur chondrules (LL3.4, Fig. 7A,B). The fayalite contents of these grains range from 9 to 40 mol% (Table 1). Concentrations of RLEs Al, Ca, Sc, Ti, V, Y and Zr in non-refractory olivine are lower by approximately a factor of 10 compared to RFs (Fig. 7). The RLE fractionation, however, is almost identical to that in RFs. Concentrations of Nb are close to or below the detection limit of LA-ICPMS (Fig. 7; Table 1).

Concentrations of Cr in ferrous olivines from Chainpur (fa_{9-15}) are similar (~1000 ppm) to those in RFs, whereas the more ferrous olivine grains from Murchison (fa_{33-40}) have Cr contents in the range of ~2500 ppm. Chainpur ferrous olivine grains show a strong Mn/Cr > $(\mathrm{Mn/Cr})_{\mathrm{C1}}$ fractionation, whereas those from Murchison show only a slight Mn/Cr > $(\mathrm{Mn/Cr})_{\mathrm{C1}}$ fractionation. Moderately siderophile elements Fe, Co and Ni are similarly fractionated in the ferrous olivines as in RFs. Concentrations levels are, however, 1–2 orders of magnitude higher than in RF grains.

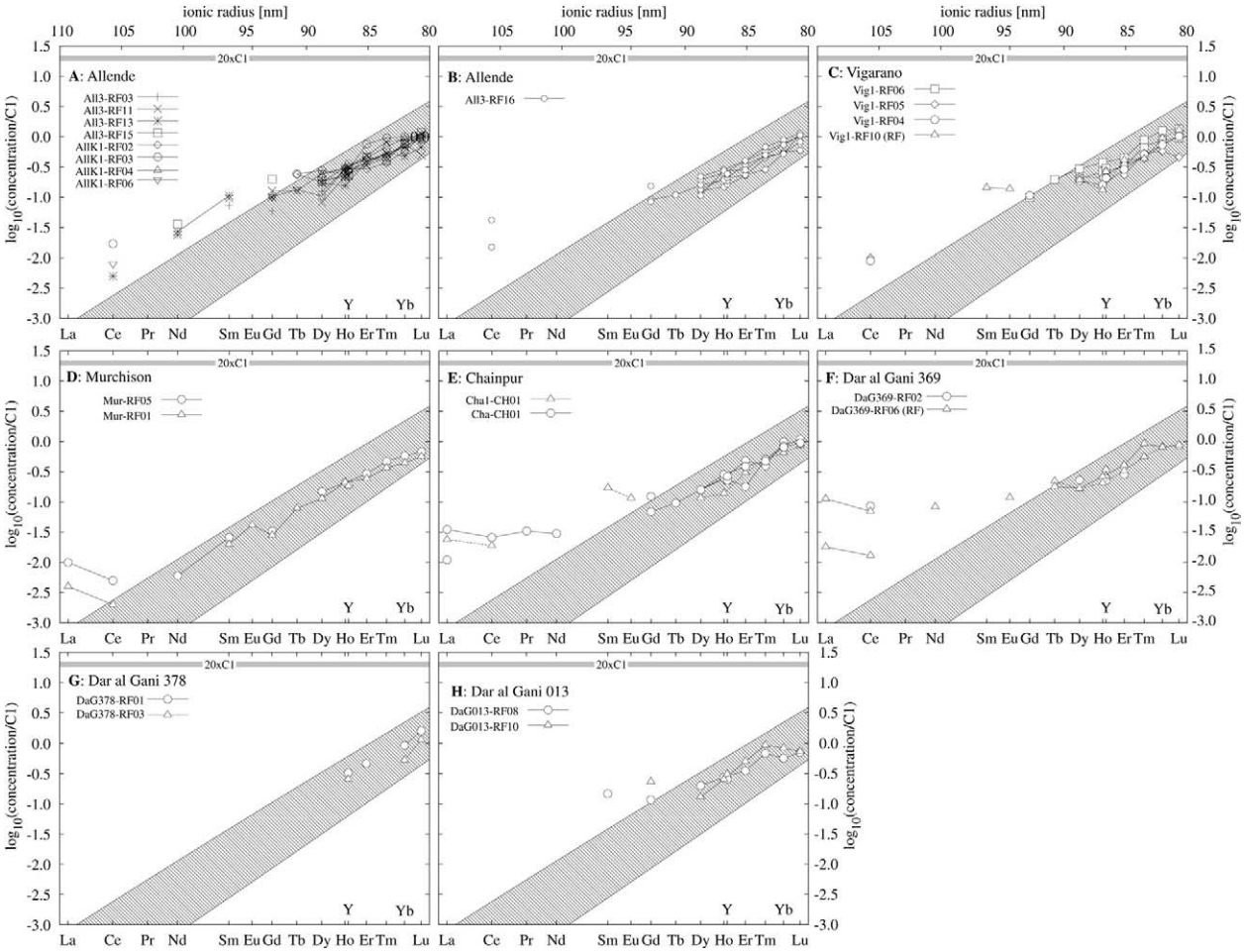

Fig. 5. C1-normalized REE and Y concentrations of RFs plotted vs. ionic radius. The hatched areas outline the calculated composition of an olivine in equilibrium with a melt with 20×C1 REEs and Y (partitioning data from Beattie, 1994).

5. DISCUSSION

5.1. Olivine/Melt Minor and Trace Element Partitioning

An igneous origin of RFs should be identifiable by systematic fractionation of minor and trace elements. If the host melt was a chondrule, RLEs are assumed to be unfractionated and the element fractionation in RFs should mirror unfractionated RLEs in the host melt. The Nernst mineral to melt partitioning coefficient (D_i) denotes the ratio of the concentration of an element i in a mineral to the concentration of the element in the coexisting melt in weight units. Using the chemical composition of RFs and available D data we have estimated the composition of a melt parental to RFs (hashed boxes in Fig. 2, Fig. 5 and Fig. 6). The uncertainty in the D data are considered by calculating the minimum value for an element in the melt by applying the minimum D to the minimum concentration of an element in the olivine. In turn, the maximum value in the olivine is combined with the maximum D.

5.2. Sources of Partitioning Data

Agee and Walker (1990) report D_{Al} for komatiitic melts at 1 atm with D_{Al} showing a dependence of the temperature between 1600 and 1300°C (open circles in Fig. 1 in Agee and Walker, 1990) with $D_{Al} = -2.509 \times \frac{10^{-3}}{T[K]} - 0.694$ ($R^2 = 0.74$). ($R^2 = 0.74$). D_{Al} decreases in the range from 1600 to 1300 °C from 0.010 to 0.0056, respectively. This is the approximate temperature range that is relevant if RFs crystallized from a silicate melt (T_{min}: ternary *fo-di-an* eutectic at 1262°C, Hytoenen and Schairer, 1961). In Figures 2A–H we have used these values as maximum and minimum D_{Al}, respectively. Partitioning data for Ca were taken from Libourel (1999) who demonstrated that D_{Ca} is solely a function of the CaO content in CMAS-Ti melts. Dynamic crystallization experiments by Pack and Palme (2003) have confirmed the relation reported by Libourel (1999) and have shown that D_{Ca} is independent of the cooling rate. The minimum to maximum D_{Ca} range of 0.025–0.037 was calculated using the empiric formula given by Libourel (1999) for CaO contents in olivine between 0.4 and 0.8 wt%. Partitioning data for Sc were taken from Kennedy et al. (1993, experiment PO49, 1525°C) and Beattie (1994). Both studies report a similar D_{Sc} between 0.12 and 0.15. D_V was taken from Kennedy et al. (1993, PO49, 1525°C) and Gaetani and Grove (1997) and range from 0.159 to 0.30. The Zr

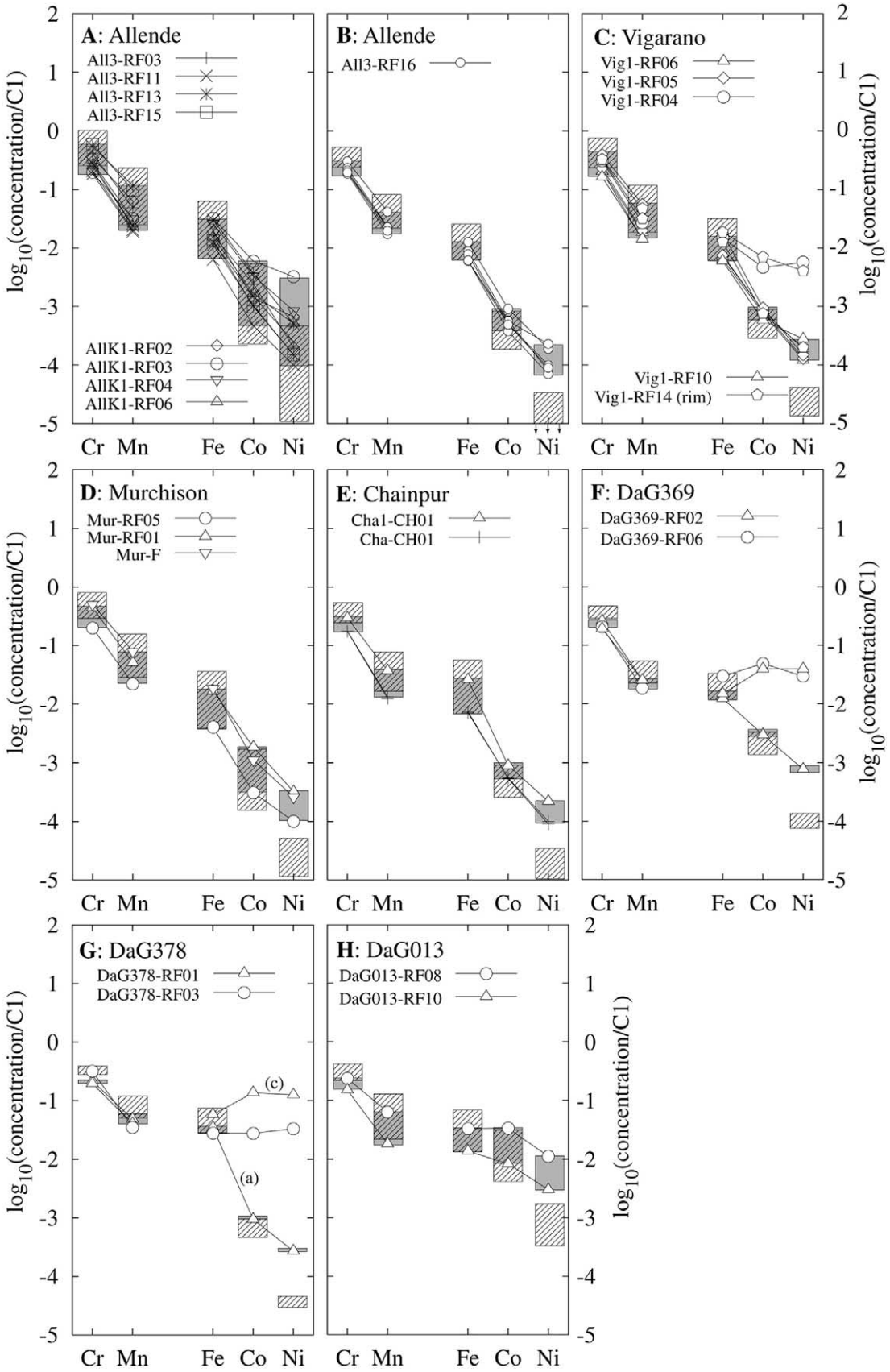

Fig. 6. Chondrite normalized concentrations of common lithophile elements Cr and Mn and moderately siderophile elements Fe, Co and Ni of RFs from different types of chondrites. The hatched boxes outline the composition of a silicate melt in equilibrium with RFs (gray boxes).

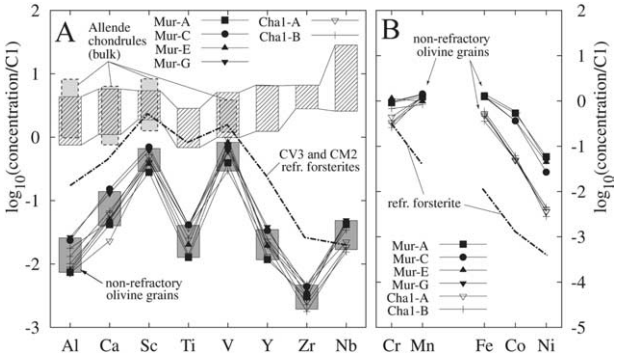

Fig. 7. C1-normalized (A) RLE and (B) Cr, Mn, Fe, Co and Ni concentrations of non-refractory olivine from Murchison (CM2, "Mur") and Chainpur (LL3.4; "Cha," gray boxes, solid outline). The hatched boxes outline the expected composition of a melt in equilibrium with non-refractory olivine. The gray boxes with the dashed outlines illustrate the compositional fields of Allende chondrules (Rubin and Wasson, 1987; Palme, unpublished INAA data). The dashed-dotted line shows the average composition of RFs.

partition coefficient was taken from Kennedy et al. (1993, experiment PO49, 1525°C) with $D_{Zr} = 0.00068$. Partition coefficients for Ti were taken from Kennedy et al. (1993, experiment PO49, 1525°C) and from Dunn and Sen (1994) with a range between 0.0142 and 0.018. D_{Nb} was taken from Dunn and Sen (1994) who report values between 0.0017 and 0.0065. Beattie (1994) reports olivine melt partitioning data for Y, La, Ce, Pr, Sm, Tb, Ho and Yb and these data were adopted for this study. The partition coefficients for those REE that were not reported by Beattie (1994) were estimated by inter and extrapolation, respectively, using a polynomial function to fit D_{REE} as function of ionic radius. In such a diagram, D_{REE} follows a smooth curve as function of the ionic radius (radii for trivalent REEs from Shannon, 1976).

Data for $D_{Cr}{}^{3+}$ (0.58–0.66) were taken from Gaetani and Grove (1997, experiment KOM). Partitioning data for Mn (D_{Mn} = 0.5–0.8) were adopted from Beattie (1994, except experiment B7), Kennedy et al. (1993, experiment PO 49) and Gaetani and Grove (1997). Partitioning data for moderately siderophile elements Fe (0.5–1.0), Co (1.1–2.2) and Ni (5.4–9) were taken from the same data sources as D_{Cr} and D_{Mn}.

5.3. RF Formation: Crystallization vs. Condensation?

RFs from different types of chondrites have similar and highly fractionated RLE patterns (Fig. 2A–H). With exception of Ti and V and considering the variability of the reported D values, these patterns can be explained in terms of equilibration with a silicate melt uniformly enriched in RLEs by ~15–20×C1 (Fig. 2A–H). Although we suggest formation of RF by crystallization from a silicate melt, we exclude FeO-poor type-I chondrules (e.g., Jones, 1992), since they contain <10×C1 RLEs (Rubin and Wasson, 1987; Palme, unpublished instrumental neutron activation [INAA] data; see also detailed discussions in Weinbruch et al., 2000; Pack and Palme, 2003 and Pack et al., 2004).

Association of isolated RF grains with low-Ca pyroxene (e.g., App. Fig. 2E) was taken by Jones (1992) as argument for derivation of RF grains from type-I chondrules. The highly refractory composition of RF grains, however, rather indicates equilibration with spinel and Al- and Ti-rich clinopyroxene than with low-Ca pyroxene. Cogenetic inclusions of spinel occur in many RF grains. We suggest that low-Ca pyroxene in association with some RFs is due to replacement of RF by low-Ca pyroxene. Replacement may either have occurred in a nebular environment by reaction with gaseous SiO in a process similar to that described by Tissandier et al. (2002) or in silica rich chondrule melts that are saturated in low-Ca pyroxene. In the latter case, RFs are relict grains and are in disequilibrium with the host chondrule.

Our interpretation of an igneous origin of RFs is supported by fractionated HREEs. Unlike the forsterites reported by Weinbruch et al. (2000), we have not found RF with chondrite normalized HREE < LREE fractionation (their grain #10). Among other arguments, Weinbruch et al. (2000) based their suggestion of formation of RF by condensation of complementarily fractionated REEs in RFs. Our REE data clearly indicate equilibration of RF with a silicate melt containing unfractionated REEs. None of the studied RFs show a negative or positive anomaly in Yb and/or Tm. Such an anomaly would be clearly supportive of formation of RFs by condensation from the gas phase (MacPherson et al., 1988; Boynton, 1989). At the condensation temperature of forsterite, however, all REEs should have condensed into solids and RF condensates may thus carry no such anomaly. Therefore, the lack of Yb and/or Tm anomalies in RFs neither supports nor contradicts a condensation origin of RF.

Non-refractory isolated and chondrule olivine grains from Murchison (CM2) and Chainpur (LL3.4) show very similar RLE fractionation patterns. The lower RLE concentrations indicate equilibration with a silicate melt with only ~1–10×C1. An origin of these olivine grains by crystallization in chondrules readily explains their RLE fractionation (Fig. 7A). In the case of non-refractory chondrule olivine grains from Chainpur, this interpretation is in agreement with textural observations that indicate in situ crystallization in chondrules. The similarity in RLE fractionation patterns between igneous non-refractory forsterite and RF supports our suggestion that RF formed by crystallization from a silicate liquid.

Concentrations of Ti in RFs suggest a host melt with 50–65×C1 Ti, which corresponds to 3.8–4.8 wt% Ti. Similarly high concentrations of Ti in the host melts to RFs were suggested by ion probe data on RF grains from Allende by Klerner (2001). Such enrichment in Ti is not known from either CAIs or chondrules. Even CAIs contain not more than ~3 wt% Ti (Allende Type-B CAI, data in Srinivasan et al., 2000). One explanation for this apparent inconsistency with an igneous formation model of RF could be the presence of Ti^{3+} at the time/location of their formation. All experimental partitioning data used for Ti considered only Ti^{4+}. If $D_{Ti}{}^{3+} > D_{Ti}{}^{4+}$, the suggested overabundance in RF host melts reflects highly reducing conditions at time/location of formation of RF with a high ratio of Ti^{3+}/Ti^{4+}. Using the relation between partitioning coefficient, charge and ionic radius (e.g., Blundy and Wood, 2003 and references therein) it is possible to estimate $D_{Ti}{}^{3+}$. Trivalent and octahedral coordinated Ti has an effective ionic radius of 67 pm, intermediate between $^{VI}Cr^{3+}$ (61.5 pm) and $^{VI}Sc^{3+}$ (73 pm, Shannon and Prewitt, 1969). Using the relation between partition coefficient (olivine/melt) and ionic radius for

trivalent cations by Beattie (1994), we suggest that D_{Ti}^{3+} is ~0.8. This value is by a factor of ~50 higher than the D_{Ti}^{4+} that we have adopted from the literature. If all Ti in the system RF/melt was trivalent and taking an average TiO_2 concentration in RF of 600 ppm, the melt compositions would then be only 1–1.3×C1. To obtain a melt composition in the range of 20×C1 Ti, ~60% of Ti in RF should be trivalent. The percentage of Ti^{3+} is insensitive to changes in D_{Ti}^{3+} towards higher numbers, whereas the Ti^{3+}/Ti^{4+} ratio should increase with decreasing D_{Ti}^{3+}. Assuming that D_{Ti}^{3+} is only 0.4, 63% of Ti should be trivalent. At $D_{Ti}^{3+} = 0.1$, ~72% of Ti should be trivalent.

The presence of 60% of Ti as Ti^{3+} would relate RFs to CAIs, which contain considerable amounts of Ti^{3+} (see Brearley and Jones, 1989 and references therein). For comparison, Lee and Greenwood (1994) report 50% of total Ti to be Ti^{3+} in Ti- and Al-rich clinopyroxene from CAIs. The presence of trivalent Ti in RF indicates formation under highly reducing conditions, similar to that under which CAIs have formed.

Concentrations of Ti in non-refractory forsterites are in agreement to crystallization from chondrules. In contrast to RFs, no anomalously high Ti is suggested for the parental melt. This shows that partitioning data for Ti^{4+} can be well applied to non-refractory chondrule olivine. The presence of Ti^{3+} in RFs clearly distinguishes these grains from chondrule olivine.

Concentrations of V in RFs from Allende, Vigarano, Murchison, DaG369 and DaG013 suggest that the host melt contained <20×C1 V with $(Al/V)_{melt} > (Al/V)_{C1}$ (Fig. 2A–D). Chondrules from Allende have $(Al/V)_{melt}/(Al/V)_{C1}$ between 0.4 and 8 with an average of 1.2 and a weak correlation between Al_{melt}/Al_{C1} and $(Al/V)_{melt}/(Al/V)_{C1}$ (Rubin and Wasson, 1987; Palme, unpublished INAA data). Hence, a chondrule that is rich in Al (and possibly other RLEs) is expected to have subchondritic V/Al. The suggested deficit in V in the RF host melts may reflect the higher volatility of V ($Tc_{50\%}$ = 1429 K) relative to Al ($Tc_{50\%}$ = 1653 K at $p_{tot} = 10^{-4}$ bar; Lodders, 2003) under solar nebula conditions.

It was shown that Ca and Al concentrations systematically decrease from core to rim in most RF grains (Pack and Palme, 2003; Pack et al., 2004; Fig. 1). Our data show the same behavior for the other RLEs, including Ti, Sc, V, Y and Zr. They all decrease from core towards the rim (Fig. 3). It was pointed out by Weinbruch et al. (2000) and Pack and Palme (2003) and Pack et al. (2004) that unzoned or decreasing concentrations of elements, which are incompatible with olivine are in disagreement with an origin by crystallization in a closed system such as a molten droplets, i.e., chondrules. Enrichment of these elements in the residual melt should lead to an increase at the rims of RF grains. Hence, our data support the model of Pack and Palme (2003) and Pack et al. (2004) that RF grains may have formed by open system fractional crystallization (OSFC) in association with melt condensates. Dilution of RLEs in the RF host melts by continuous condensation of MgO and SiO_2 and simultaneous crystallization of RFs is suggested in the OSFC model to explain the decrease in Ca and Al from core towards the rims of many RF grains. Loss of Ca and other RLEs by diffusion during parent body metamorphism could have modified the initial zoning patterns in RF grains. Fe and Ca diffusion coefficients in olivine as function of temperature were reported by Petry et al. (1999). Diffusion of Ca over a distance of x = 50 μm ($x = \sqrt{D_{Ca}^{diff} \times t}$, with D_{Ca}^{diff} being the Ca diffusion coefficient and t the time) would require ≥2.6 Ga at a temperature of $T \leq 600$°C. At T = 900°C diffusion of Ca over a distance of 50 μm would require ~500 Ma. Diffusion of Fe in olivine is by orders of magnitude faster than Ca diffusion (Petry et al., 1999). Hence, Fe should show considerably wider diffusion profiles than Ca. The opposite is observed (Fig. 1B). We therefore conclude that diffusion during parent body metamorphism did not or only negligibly alter the RLE distribution in RFs.

We suggest that RFs formed at highly reducing conditions, possibly with ~60% of the Ti present in trivalent state. Therefore the Cr^{2+} partitioning coefficient (Hanson and Jones, 1998) is used to estimate the composition of the host liquid. Hanson and Jones (1998) report D_{Cr}^{2+} of ~1 for olivine in equilibrium with low polymerized silicate melts. The concentration of Cr in the cores of RF grains (~600 ppm) may indicate equilibration with a melt containing ~600 ppm Cr. If Cr was trivalent, then its concentration in the host melt was ~900–1000 ppm. Concentrations of Cr in Allende chondrules vary between 2830 ppm and 1950 ppm (Rubin and Wasson, 1987; Palme, unpublished INAA data). A single porphyritic olivine chondrule from the data set by Rubin and Wasson (1987) shows a considerably lower Cr concentration of only 370 ppm. Concentrations of Cr are equal or slightly higher in non-refractory forsterites than in RFs. Hence our Cr data would be compatible with formation of RF by crystallization in chondrule melts.

The lower limit of Mn is at 25 ppm in Cha-CH01, suggesting a Mn concentration between 30 and 50 ppm for the host melt. Most RF grains have Mn concentrations in the range of 25–100 ppm, suggesting a host melt with 30–200 ppm Mn. Our data are in good agreement with previous studies which report a lower limit of 30 ppm in RF from Allende (Weinbruch et al., 1993a). The lower limit of Mn in chondrules from Allende is between 410 ppm (Rubin and Wasson, 1987) and 370 ppm (Palme, unpublished INAA data) and is by a factor of >10 too high to be parental to RF. Rubin and Wasson (1988) report minimum values of 660 ppm Mn in CO chondrules. The low concentration of Mn hence excludes formation of RF by crystallization in type-I chondrules (see also Weinbruch et al., 2000). Low Mn concentrations in RFs suggest an origin in a high-T environment at >1158 K ($T_{c50\%}$ of Mn, $p_{tot} = 10^{-4}$ bar, Lodders, 2003) in which the condensed phases were strongly depleted in Mn. Concentrations of Mn in non-refractory olivine grains are more than one order of magnitude higher than in RFs and are in agreement with formation by crystallization from a chondrule melt. The higher Mn/Cr ratios in non-refractory olivine of Chainpur compared to Murchison (Fig. 7A) clearly relate these olivine grains to their host meteorites. OCs have higher bulk Mn/Cr ratios than CCs chondrites (Jarosewich, 1990).

Fractionated moderately siderophile elements cannot be explained in terms of equilibration with a melt with unfractionated Fe, Co and Ni since D increases from Fe to Co and Ni. An olivine crystallizing from a silicate melt with chondritic Fe, Co and Ni would have, normalized to C1, ~10× more Ni than Fe. The minimum values for FeO, Co and Ni are 0.15 wt%, 0.2 ppm and 0.7 ppm, respectively. Our lower limits in Co and Ni are slightly lower than those reported by Weinbruch et al.

(1993a, 2000). If RFs crystallized from silicate melts these concentrations suggest a melt composition with ~0.2 wt% FeO, ~0.1 ppm Co and ~0.1 ppm Ni. The lowest concentration of Co in Allende chondrules is 15 ppm and of Ni 170 ppm, respectively (Palme, unpublished INAA data). If all Co and Ni are present as oxides only, concentrations are by factors of 150 and 1700, respectively, too high to crystallize RF.

An explanation for the fractionated moderately siderophile elements is equilibration with Fe,Ni-metal. The decreasing C1-normalized abundance from Fe to Ni would then reflect the increasing degree of the siderophile character from Fe to Co and Ni. Seifert et al. (1988) report Fe/Co and Fe/Ni partitioning data between olivine (~20 mol% fayalite) and solid ternary Fe,Co,Ni-metal alloys. Equilibration at 1273 K would suggest a metal with ~2×C1 Co/Fe for those olivine grains with <1 ppm Co and ~4×C1 Ni/Fe for olivine with <4 ppm Ni. At 1673 K metal in equilibrium with RF with <1 ppm Co and <4 ppm Ni would contain ~1.2×C1 Co and ~2×C1 Ni/Fe, respectively. The suggested metal composition (T = 1673 K) resembles the composition of metal condensates (Petaev et al., 2003).

In the case of equilibration of RF with primitive metal, low concentrations of Fe, Co and Ni in RF would reflect the highly reducing conditions during their formation. Ehlers et al. (1992) report Ni partitioning data between olivine and metal and its dependence of the oxygen fugacity at a temperature of 1350°C. Using the estimated composition of metal (~10 wt.% Ni) in equilibrium with RF (1 ppm Ni) for 1623 K ($D_{Ni}^{ol\text{-}melt} \approx 10^{-5}$), an oxygen fugacity of $f_{O2} = 10^{-16.2}$ is calculated. At 1623 K a gas of solar composition buffers an oxygen fugacity of $f_{O2} = 10^{-16.6}$ (Krot et al., 2000). Hence, RFs with their low concentrations of moderately siderophile elements may have formed in equilibrium with primitive metal at approximately solar nebular oxygen fugacity. Olivine and metal compositions from the experiments by Ehlers et al. (1992) and Seifert et al. (1988), however, deviate from the composition of RF and metal in equilibrium with it. The Fe,Ni-alloy that was used by Ehlers et al. (1992) was very Ni-rich (40 and 64 wt.% Ni) and the olivine was more ferrous (4.8 and 9.5 wt.% FeO) than RF. Seifert et al. (1988) equilibrated olivine ($fa_{\sim 20}$) with Fe,Ni,Co-metal with ~4–40 mol% Ni. Therefore, the given f_{O2} may be considered as estimate with an uncertainty in the range of 0.5–1 order of magnitude.

Those RF grains that have largely unfractionated Fe, Co and Ni (Fig. 6C, 6F, 6G) may have acquired their pattern from metal inclusions. Since we have not observed metal inclusions in these grains, we suggest that these inclusions are either submicroscopically small or that they have been oxidized and that FeO, CoO and NiO have been quantitatively been incorporated into the olivine. Both processes would ultimately lead to analyses with unfractionated Fe, Co and Ni.

From olivine to melt partitioning data we infer a host melt with ~20 wt.% Al_2O_3 (olivine can only crystallize in CMAS systems with <25 wt.% alumina), ~20 wt.% CaO (to obtain forsterite with ~0.6 wt.% CaO, Libourel, 1999; Pack and Palme, 2003), ~1.5 wt.% TiO_2, ~0.5 wt.% FeO. In addition, we suggest ~44 wt.% SiO_2 and ~14 wt.% MgO to adjust the melt composition so that it is saturated in forsterite.

Normal olivine grains (Fig. 7B) show also C1-normalized fractionated Fe > Co > Ni that indicates metal fractionation. Concentrations of Fe, Co and Ni are, however, 1–2 orders of magnitude higher and indicate separation of metal at higher oxygen fugacity and/or lower temperature.

5.4. Origin of RF Host Melts

Our major, minor and trace element data show that RF grains from different types of chondrites have formed by crystallization from RLE- and REE-rich melts that were poor in oxidizable siderophile elements (Fe, Co, Ni) and very poor in Mn. These melts were intermediate in chemical and oxygen isotope composition between CAIs and chondrules. Varela et al. (2002), Pack and Palme (2003) and Pack et al. (2004) have suggested that RF grains have formed in association with refractory melt condensates. However, so far there is little unequivocal evidence for the presence of melt condensates, such as suggested by Ebel and Grossman (2000). High dust/gas ratios are necessary to condense melts (Ebel and Grossman, 2000). These, however, lead to an oxygen fugacity that is higher than buffered by a gas of solar composition and consequently to high FeO concentrations in the silicates. Our data indicate that RF grains have formed in equilibrium with a gas of approximately solar composition. Either melt condensates are stable also at lower dust/gas ratios as suggested by Ebel and Grossman (2000; see discussion in Pack and Palme, 2003) or the host melts to RFs did not form by condensation. Tachibana et al. (2003), based on ^{26}Mg–^{26}Al chronology, suggested that less refractory chondrules are younger than more refractory chondrules. The interpretation that RF grains have formed within the very first generation of chondrules is in agreement to the observation by Tachibana et al. (2003). These chondrules must have been very RLE- and REE-rich and poor in moderately siderophile elements. They must have formed in equilibrium with a gas of solar composition and high ambient temperatures, as indicated by deficits in V and Mn. If chondrule recycling was as effective as suggested by Alexander (1995), most of early chondrules have been incorporated as parts of later chondrules. Zanda et al. (2004) report luminescent Ca- and Al-rich RF bars in an Allende (CV3) barred olivine chondrule. In this chondrule RF is associated with spinel and Al-rich pyroxene. In terms of bulk chemical composition, this chondrule may be close to the suggested composition of the RF host melt. Decreasing RLEs in RF grains, however, cannot be explained in terms of closed system crystallization and require open system behavior of these chondrules (Pack et al., 2004).

The origin of RF grains from amoeboid olivine aggregates (AOAs) shall briefly be discussed. Forsteritic, ^{16}O rich olivine is a major phase of AOAs (see Krot et al., 2004). Thus there may be a relationship between RF and forsterites of AOAs. AOA olivine is usually FeO-poor and is reported to contain up to 0.8 wt.% CaO (Krot et al., 2004) and would hence have a composition similar to RF. The large size of RF grains would require melting of an AOA and crystallization of coarse-grained olivine. Melting of AOAs in a nebular environment with $\Delta^{17}O \geq -10‰$ (e.g., during chondrule formation) would readily explain the oxygen isotope ratios of RFs, which are less ^{16}O rich than AOA olivine (Pack et al., 2004; Table 1). Bulk AOAs, however, are usually too poor in CaO to crystallize RF

with high Ca (Grossman et al., 1979; Komatsu et al., 2001), although a chemical continuum between Ca poor AOAs and Ca rich CAIs is apparent. Partial melting of AOAs can result in highly refractory silicate melts, which could be parental to RFs. Low concentrations of Mn in RFs would require formation from an AOA with <100 ppm Mn. AOA in Allende (CV3) have bulk Mn concentrations between 560 and 1800 ppm (Grossmann et al., 1979). As for Fe, partial melting would concentrate Mn in the liquid. Decreasing RLEs from core to rim are difficult to explain in any closed system crystallization process (e.g., in chondrules or partially molten AOAs). It is thus concluded that RF grains did probably not simply originate from partially molten AOAs.

Many of the arguments that were presented to explain formation of RF by crystallization within refractory silicate melts may also apply to formation by condensation. Weinbruch et al. (2000) summarized a number of *pros* and *contras* for an origin of RF by crystallization and eventually suggest formation of RF by condensation. Although no gas to olivine partitioning data are currently available, olivine condensates will likely show preference for certain elements, while others will be rejected. Olivine in equilibrium with other condensates (pyroxene, spinel, feldspar) will show a preference for HREEs, whereas remaining LREEs may enter coexisting phases, irrespective of the surrounding environment (solar nebula vs. silicate melt). The resultant minor and trace element pattern in olivine may resemble those described in this study. We interpret the occurrence of glass inclusions in RFs from different types of meteorites, however, as clear indication that silicate liquids were present (Fuchs et al., 1973; McSween, 1977; Roedder, 1981; Steele, 1991; Weinbruch et al., 2000). This implies that RF formed in equilibrium with a refractory silicate melt during their formation.

To unambiguously distinguish between an origin by condensation and an origin by crystallization in a liquid, it would be very informative to include trace element solid solutions in silicates (e.g., Palme and Fegley, 1990) and oxides in existing full condensation codes (Ebel and Grossman, 2000; Lodders, 2003). Minor and trace element condensation models were successfully applied to the problem of formation of CH chondrite metal grains (e.g., Campbell and Humayun, 2004). Also micro-structural differences between vapor and melt grown minerals could bear additional information about the origin of chondritic RFs.

6. SUMMARY

RFs from different types of unequilibrated chondrites (CV, CM, L/H, R) have similarly fractionated RLE and REE patterns. This suggests that RFs from different types of chondrites formed by the same process, possibly from a single reservoir. Our data support the interpretation by Steele (1986a, 1986b) who compared RF grains from carbonaceous and ordinary chondrites and suggested formation from a common reservoir. We suggest that the RLE and REE fractionation are the result of equilibration with a refractory element rich silicate melt with ~15–20×C1 RLEs and REEs. The presence of glass inclusions in RFs (McSween, 1977; Roedder, 1981; Steele, 1991; Varela et al., 2002) supports their igneous origin. The melt clearly was more refractory than type-I chondrules and may have been in composition intermediate between chondrules and CAIs.

The enrichment of many RFs in ^{16}O (Weinbruch et al., 1993b; Leshin et al., 1997; Pack et al., 2004 and references therein) supports an origin from material intermediate between chondrules and CAIs that are typically enriched in ^{16}O (Clayton et al., 1977).

Fractionation of the moderately siderophile elements Fe, Co and Ni in RFs is compatible with formation in equilibrium with primitive metal with slightly enhanced Ni/Fe and Co/Fe ratios, respectively. Such metal compositions are suggested for metal condensates. The low concentration of Fe, Co and Ni suggest formation at low oxygen fugacity in equilibrium with a gas of solar composition. Formation at low f_{O2} is also supported by the presence of Ti^{3+} in RF grains.

Varela et al. (2002), Pack and Palme (2003) and Pack et al. (2004) suggested formation of RF by crystallization from condensed refractory element rich melts. Condensation calculations by Ebel and Grossman (2000) show that condensed melts would be rich in RLE and poor in moderately volatile elements. They are therefore appropriate candidates for producing RF during crystallization, as discussed in Pack and Palme (2003) and Pack et al. (2004). Alternatively, RF grains may have formed in a very first generation of RLE-rich chondrules. Traces of these chondrules would have been erased during chondrule recycling and only large RF grains could survive this process.

The data presented here and in earlier papers demonstrate that there was either a single source of nebular origin for all RFs parental to the different types of chondrites or that the formation location of the various classes of chondritic meteorites were in the beginning very similar, implying similar oxygen isotopes, and only processes at lower temperature led to the diversification of chondritic meteorites. In both cases chondrite formation cannot be achieved within a closed system. Transport of RFs to the various chondrite formation locations is required in the first case and addition of gases with variable composition is necessary in the second case.

Acknowledgments—J. Zipfel (MPI, Mainz) is thanked for loaning the thin sections of Dar al Gani 369 and Dar al Gani 378, A. Bischoff (University of Münster) for this section of Dar al Gani 013 and R. Schumacher (University of Bonn) for the sections of Vigarano. C. M. Allen (ANU Canberra) is thanked for her help and fruitful discussions concerning LA-ICPMS data reduction. H. St. O'Neill and D. Kelly (ANU Canberra) are thanked for their support during the stay of A. P. at ANU. Inspiring discussions with G. Libourel (Nancy), D. Hezel and T. Schönbeck (both Cologne) are greatly appreciated. Constructive contributions of two anonymous reviewers and the A.E. led to substantial improvement of the manuscript. This work was funded by the German Science Foundation (DFG) through grants PA 346/24 1 (H. P.) and PA-909/1–1 (A. P., DFG Emmy Noether-Program).

Associate editor: S. R. Russell

REFERENCES

Agee C. B. and Walker D. (1990) Aluminum partitioning between olivine and ultrabasic silicate liquid to 6 GPa. *Contr. Min. Petr.* **105,** 243–254.

Alexander C. M. O'D. (1995) Trace element contents of chondrule rims and interchondrule matrix in ordinary chondrites. *Geochim. Cosmochim. Acta* **59,** 3247–3266.

Beattie P. (1994) Systematics and energetics of trace-element partitioning between olivine and silicate melts: implications for the nature of mineral/melt partitioning. *Chem. Geol.* **117,** 57–71.

Bischoff A. (2000) Mineralogical characterization of primitive, type-3 lithologies in Rumuruti chondrites. *Meteor. Planet. Sci.* **35,** 699–706.

Blundy J. and Wood B. (2003) Partitioning of trace elements between crystals and melts. *Earth Planet. Sci.* **210,** 383–397.

Boynton W. V. (1989) Cosmochemistry of the rare earth elements: condensation and evaporation processes. In *Geochemistry and mineralogy of rare earth elements* (eds. B. R. Lipin and G. A. McKay), pp. 1–24. Min. Soc. Am, Washington.

Brearley A. J. and Jones R. H. (1989) Chondritic meteorites. In *Planetary Materials* (ed. J. J. Papike), pp. 3æ1–3–398. Min. Soc. Am, Washington.

Campbell A. E. and Humayun M. (2004) Formation of metal in the CH chondrites ALH 85085 and PCA 91467. *Geochim. Cosmochim. Acta* **68,** 3409–3422.

Clayton R. N., Onuma N., Grossman L. and Mayeda T. K. (1977) Distribution of the pre-solar component in Allende and other carbonaceous chondrites. *Earth Planet. Sci. Lttrs.* **34,** 209–224.

Dunn T. and Sen C. (1994) Mineral/matrix partition coefficients for orthopyroxene, plagioclase and olivine in basaltic to andesitic systems: a combined analytical and experimental study. *Geochim. Cosmochim. Acta* **58,** 717–733.

Ebel D. S. and Grossman L. (2000) Condensation in dust-enriched systems. *Geochim. Cosmochim. Acta* **64,** 339–366.

Ehlers K., Grove T. L., Sisson T. W., Recca S. I. and Zervas D. (1992) The effect of oxygen fugacity on the partitioning of nickel and cobalt between olivine, silicate melt and metal. *Geochim. Cosmochim. Acta* **56,** 3733–3743.

Fuchs L. H., Olsen E. and Jensen K. J. (1973) Mineralogy, mineral-chemistry and composition of the Murchison (C2) meteorite. *Smith. Contrib. Earth Sci.* **10,** 1–39.

Gaetani G. A. and Grove T. L. (1997) Partitioning of moderately siderophile elements among olivine, silicate melt and sulfide melt: constraints on core formation in the Earth and Mars. *Geochim. Cosmochim. Acta* **61,** 1829–1846.

Grossman L. (1972) Condensation in the primitive solar nebula. *Geochim. Cosmochim. Acta* **36,** 597–620.

Grossman L., Ganapathy R., Methot R. L. and Davis A. M. (1979) Trace elements in the Allende meteorite—IV. Amoeboid olivine aggregates. *Geochim. Cosmochim. Acta* **43,** 817–829.

Hanson B. and Jones J. H. (1998) The systematics of Cr^{3+} and Cr^{2+} partitioning between olivine and liquid in the presence of spinel. *Am. Min.* **83,** 669–684.

Hytoenen K. and Schairer J. F. (1961) The plane enstatite-anorthite-diopside and its relation to basalts. *Year Book—Carneg. Inst.* **60,** 125–141.

Jarosewich E. (1990) Chem. analyses of meteorites: a compilation of stony and iron meteorite analyses. *Meteor.* **25,** 323–227.

Jones R. H. (1992) On the relationship between isolated and chondrule olivine grains in carbonaceous chondrite ALHA77307. *Geochim. Cosmochim. Acta* **56,** 467–482.

Jones, R. H. and Scott, E. D. (1989) Petrology and thermal history of Type-IA chondrules from Semarkona (LL3.0) chondrite. *Proc. Lun. Planet. Sci. Conf.* **IX,** Houston, 523–536.

Kennedy A. K., Lofgren G. E. and Wasserburg G. J. (1993) An experimental study of trace element partitioning between olivine, orthopyroxene and melt in chondrules: equilibrium values and kinetic effects. *Earth Planet. Sci. Lttrs.* **115,** 177–195.

Klerner S., Jones R. H., Palme H. and Shearer C. K. (2000) Trace elements and cathodoluminescence in refractory forsterite from Allende and Kaba. *Lun. Planet. Sci.* **XXXI,** Lun. Planet. Inst., Houston, #1689 (abstract).

Klerner S. (2001) Materie im frühen Sonnensystem: Die Entstehung von Matrix, Chondren und refraktärem Forsterit. PhD-thesis, Universität zu Köln, 119 p.

Komatsu M., Krot A. N., Petaev M. I., Ulyanov A. A., Keil K. and Miyamoto M. (2001) Mineralogy and petrography of amoeboid olivine aggregates from the reduced CV3 chondrites Efremovka, Leoville and Vigarano: products of nebular condensation, accretion and annealing. *Meteor. Planet. Sci.* **36,** 629–641.

Krot A. N., Fegley B., Lodders K. and Palme H. (2000) Meteoritical and astrophysical constraints on the oxidation state of the solar nebua. In *Protostars and planets IV* (eds. V. Mannings, A. Boss and S. S. Russell), pp. 1019–1054. Univ. of Arizona Press, Tucson.

Krot A. N., Petaev M. I., Russell S. S., Itoh S., Fagan T. J., Yurimoto H., Chizmadia L., Weisberg M. K., Komatsui M., Ulyanovj A. A. and Keil K. (2004) Amoeboid olivine aggregates and related objects in carbonaceous chondrites: records of nebular and asteroid processes. *Chemie der Erde* **64,** 185–239.

Lee M. R. and Greenwood R. C. (1994) Alteration of calcium- and aluminum-rich inclusions in the Murray (CM2) carbonaceous chondrite. *Meteor.* **29,** 780–790.

Leshin L. A., Rubin A. E. and McKeegan K. D. (1997) The oxygen isotopic composition of olivine and pyroxene from C1 chondrites. *Geochim. Cosmochim. Acta* **61,** 835–845.

Libourel G. (1999) Systematics of calcium partitioning between olivine and silicate melt: implications for melt structure and calcium content of magmatic systems. *Contr. Min. Petr.* **136,** 63–80.

Lodders K. (2003) Solar system abundaces and condensation temperatures of the elements. *Astrophys. J.* **591,** 1220–1247.

Longerich H. P., Jackson S. E. and Günther D. (1996) Laser ablation inductively coupled plasma mass spectrometric transient signal data acquisition and analyte concentration calculation. *J. Anal. Atom. Spectr.* **11,** 899–904.

MacPherson G. J., Wark D. and Armstrong J. T. (1988) Primitive materials surviving in chondrites: Refractory inclusions. In *Meteorites and the Early Solar System* (eds. J. Kerridge and M.S. Matthews), pp. 746–807. Univ. of Arizona Press.

McSween H. Y., Jr. (1977) On the nature and origin of isolated olivine grains in carbonaceous chondrites. *Geochim. Cosmochim. Acta* **41,** 411–418.

Meibom A., Petaev M. I., Krot A. N., Wood J. A. and Keil K. (1999) Primitive FeNi metal grains in CH carbonaceous chondrites formed by condensation from a gas of solar composition. *J. Geophys. Res.* **104,** 22053–22060.

Norman M. D., Pearson N. J., Sharma, A. and Griffin W. L. (1996) Quantitative analysis of trace elements in geological materials by laser ablation ICPMS: instrumental operating conditions and calibration values of NIST glasses. *Geostand. News.* **20,** 247–261.

Pack A. and Palme H. (2003) Partitioning of Ca and Al between forsterite and silicate melt in dynamic systems with implications for the origin of Ca, Al-rich forsterites in primitive meteorites. *Meteor. Planet. Sci.* **38,** 1263–1281.

Pack A., Yurimoto H. and Palme H. (2004) Petrographic and oxygen-isotopic study of refractory forsterites from R-chondrite Dar al Gani 013 (R3.5–6), unequilibrated ordinary and carbonaceous chondrites. *Geochim. Cosmochim. Acta* **68,** 1135–1157.

Palme H. and Fegley B., Jr. (1990) High-temperature condensation of iron-rich olivine in the solar nebula. *Earth Planet. Sci. Lett.* **101,** 180–195.

Pearce N. J. G., Perkins W. T., Westgate J. A., Gorton M. P., Jackson S. E., Neal C. R. and Chenery S. P. (1997) A compilation of new and published major and trace element data for NIST SRM 610 and NIST SRM 612 glass reference materials. *Geostand. News.* **21,** 115–144.

Petaev M. I., Wood J. A., Meibom A., Krot A. N. and Keil K. (2003) The ZONET thermodynamic and kinetic model of metal condensation. *Geochim. Cosmochim. Acta* **67,** 1737–1751.

Petry C, Chakraborty S. and Palme H. (1999) Ni, Fe-olivine exchange thermometer and diffusion coefficients in olivine as a tool for determining the thermal history of meteorite parent bodies. *Lun. Planet. Sci.* **XXX,** Lun. Planet. Inst., Houston, #1248 (abstract).

Richardson S. M. and McSween H. Y., Jr. (1978) Textural evidence bearing on the origin of isolated olivine crystals in C2 carbonaceous chondrites. *Earth Planet. Sci. Lett.* **37,** 485–491.

Rocholl A. (1998) Major and trace element composition and homogeneity of microbeam reference material: basalt glass USGS BCR-2G. *Geostand. News.* **22,** 33–45.

Roedder E. (1981) Significance of Ca-Al-rich silicate melt inclusions in olivine crystals from the Murchison type II carbonaceous chondrite. *Bull. Minéral.* **104,** 339–353.

Rubin A. E. and Wasson J. T. (1987) Chondrules, matrix and coarse-grained chondrule rims in the Allende meteorite: origin, interrela-

tionship and possible precursor components. *Geochim. Cosmochim. Acta* **51,** 1923–1937.

Rubin A. E. and Wasson J. T. (1988) Chondrules and matrix in the Ornans CO3 meteorite—possible precursor components. *Geochim. Cosmochim. Acta* **52,** 425–432.

Seifert S., O'Neill H. St. C. and Brey G. (1988) The partitioning of Fe,Ni and Co between olivine, metal and basaltic liquid—an experimental and thermodynamic investigation, with application to the composition of the lunar core. *Geochim. Cosmochim. Acta* **52,** 603–616.

Shannon, R. D. and Prewitt, C. T. (1969) Effective ionic radii in oxides and fluorides, *Acta Cryst*. **B25,** 925–946.

Shannon, R. D. (1976) Revised effective ionic radii in halides and chalcogenides, *Acta Cryst*. **A32,** 751–767.

Srinivasan G., Huss G. R. and Wasserburg G. J. (2000) A petrographic, chemical and isotope study of calcium-aluminum-rich inclusions and aluminum-rich chondrules from the Axtell (CV3) chondrite. *Meteor. Planet. Sci.* **35,** 1333–1354.

Steele I. M., Smith J. V. and Skirius C. (1985) Cathodoluminescence zoning and minor elements in forsterites from the Murchison (CM2) carbonaceous chondrite. *Nature* **313,** 294–297.

Steele I. M. (1986a) Compositions and textures of relict forsterite in carbonaceous and unequilibrated ordinary chondrites. *Geochim. Cosmochim. Acta* **50,** 1379–1395.

Steele I. M. (1986b) Cathodoluminescence and minor elements in forsterites from extraterrestrial samples. *Am. Min.* **71,** 966–970.

Steele I. M. (1989) Composition of isolated forsterites in Ornans (C3O). *Geochim. Cosmochim. Acta* **53,** 2069–2079.

Steele I. M (1991) High resolution scanning ion probe imaging and analysis of submicron inclusions in meteoritic forsterite. *Lun. Plan. Sci.* **XXII,** 1325–1326 (abstract).

Tachibana S., Nagahara H., Mostefaoui S. and Kita N. T. (2003) Correlation between relative ages inferred from ^{26}Al and bulk compositions of ferromagnesian chondrules in least equilibrated ordinary chondrites. *Meteor. Planet. Sci.* **38,** 939–962.

Tissandier L., Libourel G. and Robert F. (2002) Gas-melt interactions and their bearing on chondrule formation. *Meteor. Planet. Sci.* **37,** 1377–1389.

Varela M. E., Kurat G., Hoppe P. and Brandstätter F. (2002) Chemistry of glass inclusions in olivines of the CR chondrites Renazzo, Acfer 182, and El Djouf 001. *Geochim. Cosmochim. Acta* **66,** 1663–1679.

Wasson J. T. and Rubin A. E. (2003) Ubiquitous low-FeO relict grains in type II chondrules and limited overgrowths on phenocrysts following the final melting event. *Geochim. Cosmochim. Acta* **67,** 2239–2250.

Weinbruch S., Palme H., Müller G. and El Goresy A. (1990) FeO-rich rims and veins in Allende forsterite: Evidence for high temperature condensation at oxidizing conditions. *Meteor.* **25,** 115–125.

Weinbruch S., Specht S. and Palme H. (1993a) Determination of Fe, Mn, Ni and Sc in olivine by secondary ion mass spectrometry. *Eur. J. Mineral.* **5,** 37–41.

Weinbruch S., Zinner E. K., El Goresy A., Steele I. M. and Palme H. (1993b) Oxygen isotopic composition of individual olivine grains from the Allende meteorite. *Geochim. Cosmochim. Acta* **57,** 2649–2661.

Weinbruch S., Palme H. and Spettel B. (2000) Refractory forsterite in primitive meteorites: condensates from the solar nebula? *Meteor. Planet. Sci.* **35,** 161–171.

Zanda B., Libourel G. and Blanc, P (2004) Source chondrules for refractory forsterites in primitive chondrites. *Meteor. Planet. Sci.* (in revisions).

APPENDIX

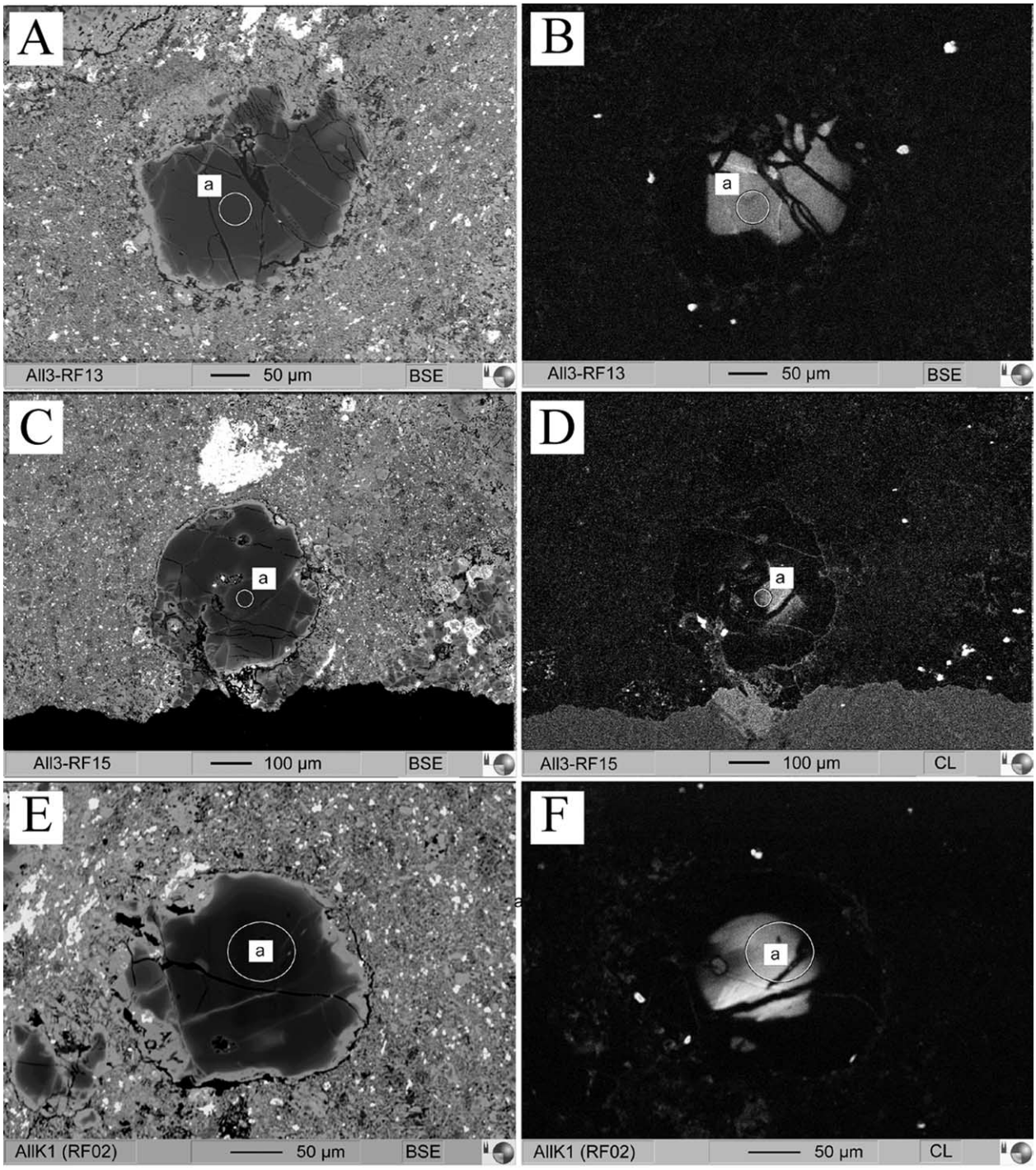

App. Fig. 1. BSE and corresponding CL images of RFs from carbonaceous chondrite Allende (A–J). Positions of LA-ICPMS spots are indicated.

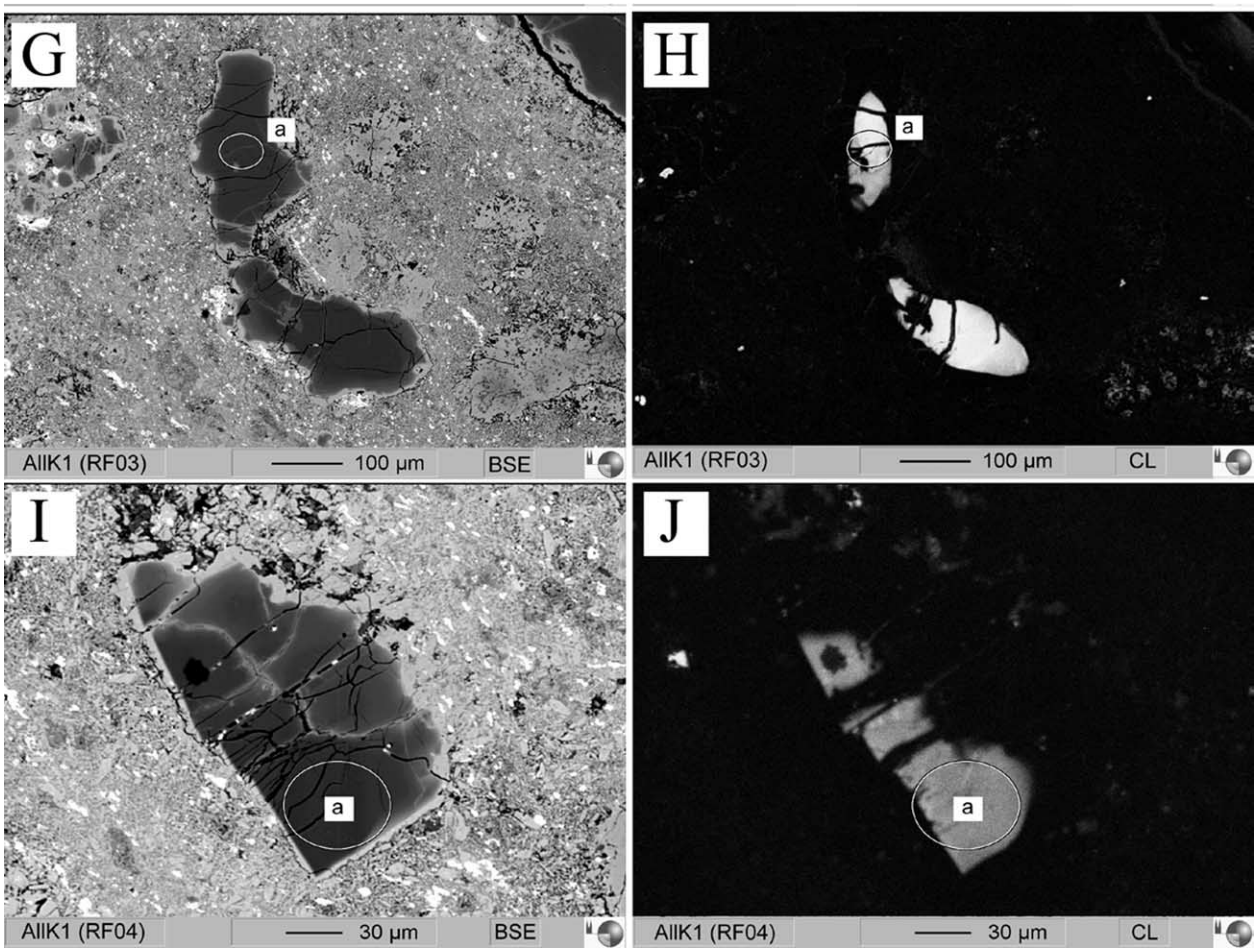

App. Fig. 1. (Continued)

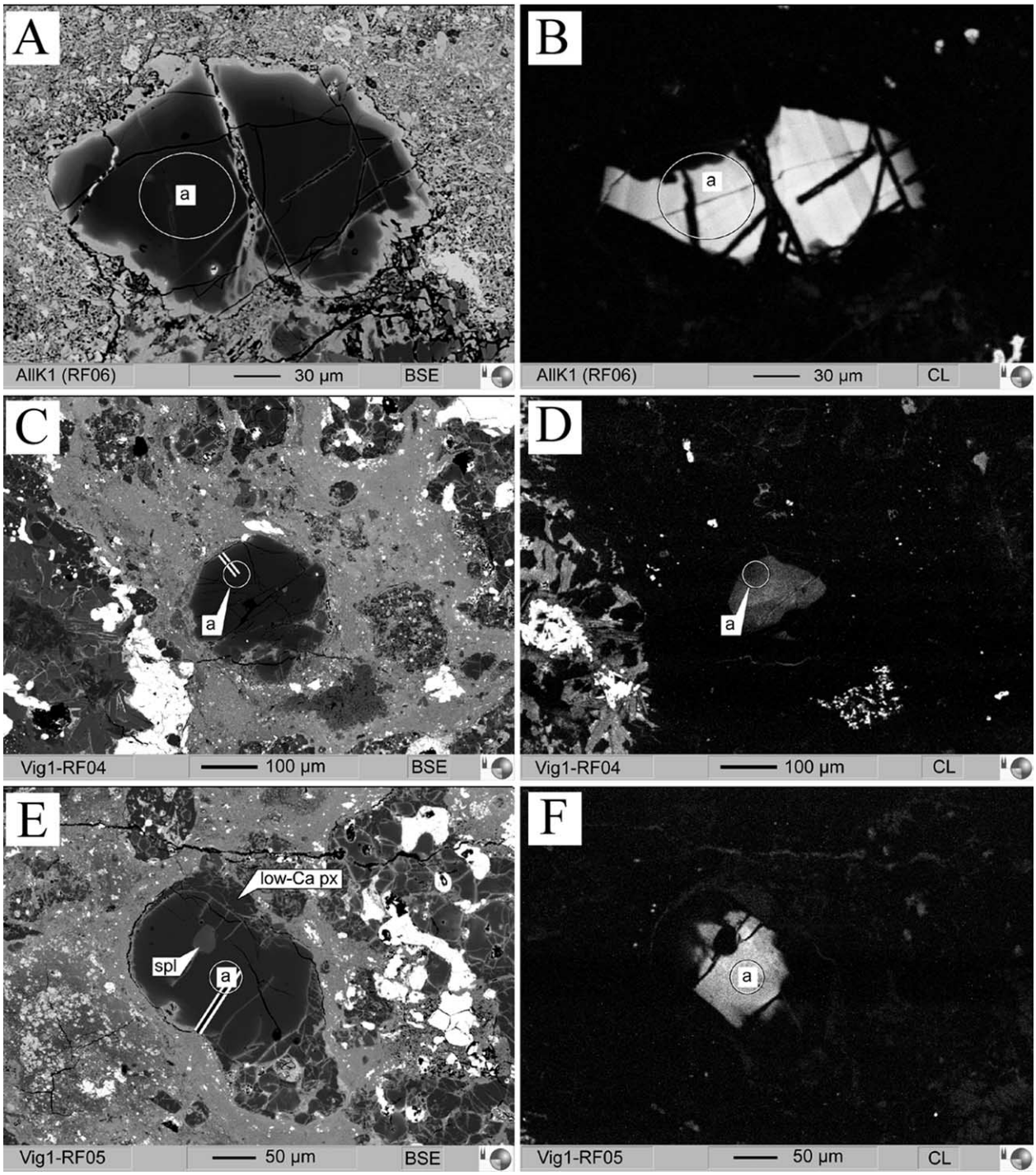

App. Fig. 2. BSE and corresponding CL images of RFs from carbonaceous chondrites Allende (A, B) and Vigarano (C–J). Positions of EPMA profiles (C, E, I) and LA-ICPMS spots are indicated.

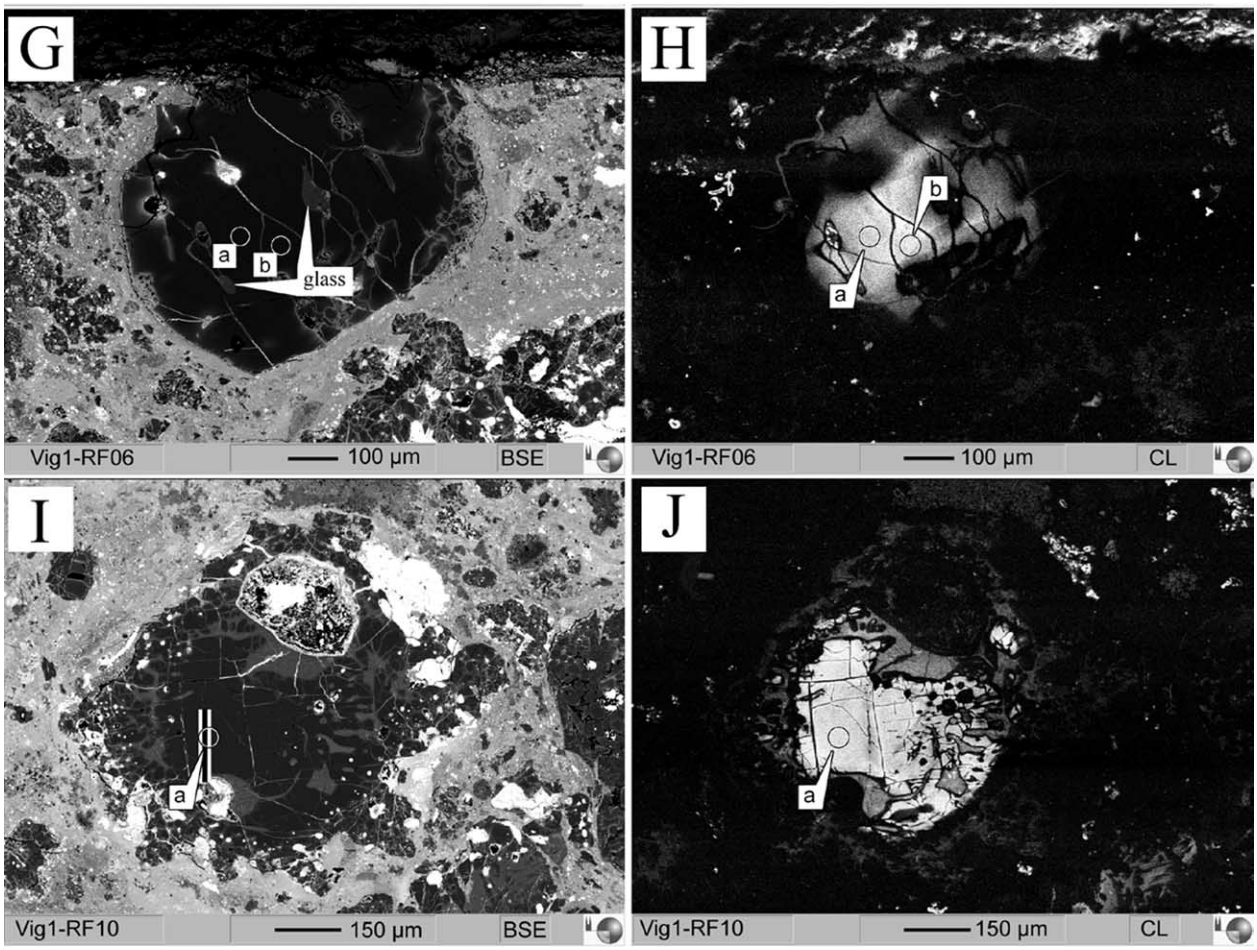

App. Fig. 2. (Continued)

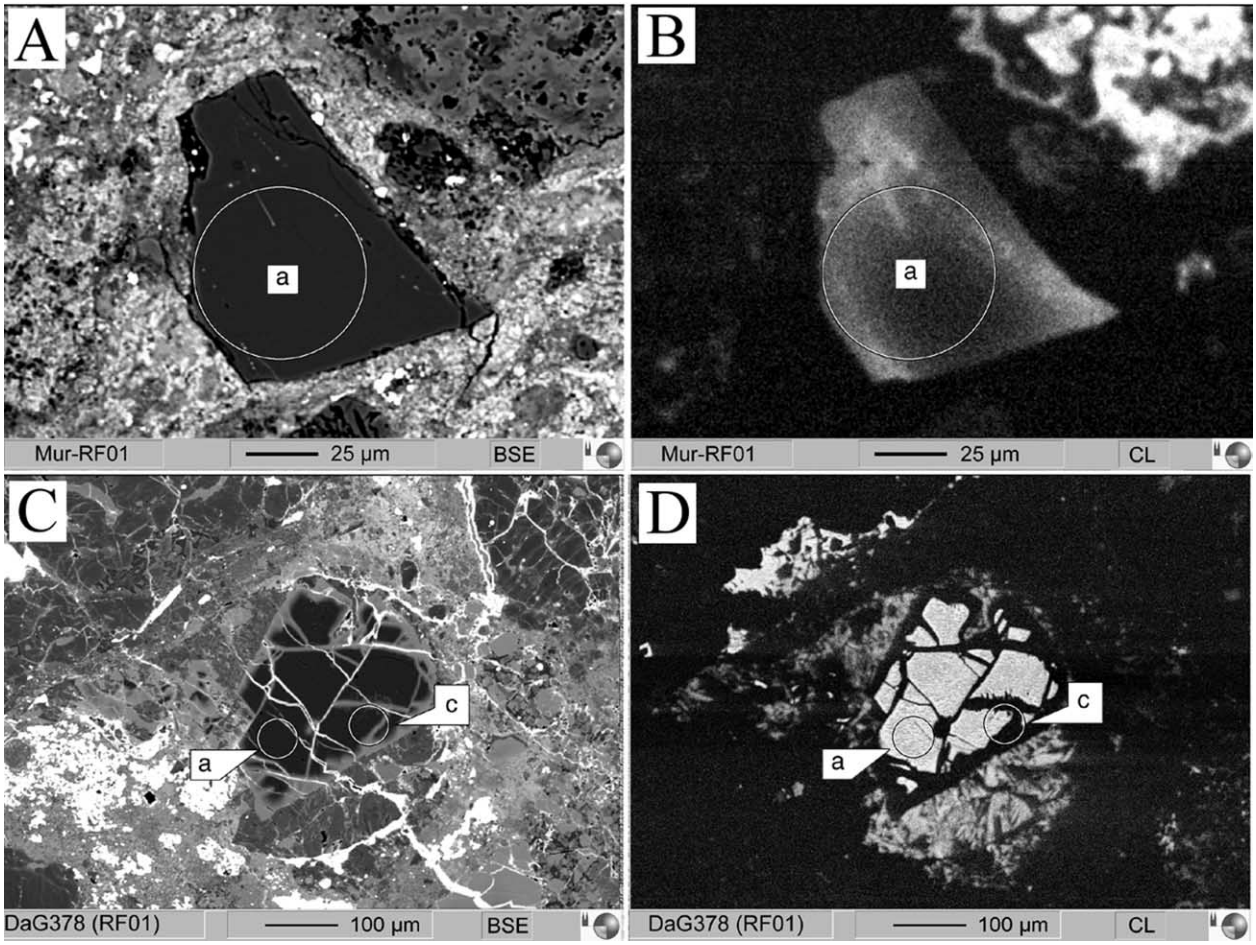

App. Fig. 3. BSE and corresponding CL images of RFs from carbonaceous chondrite Murchison (A, B) and from ordinary chondrite Dar al Gani 378 (C, D). Positions of LA-ICPMS spots are indicated.